CHAPTER IV
RESULTS AND DISCUSSION

This chapter is divided into two parts namely, propylene glycol conversion and pinacol rearrangement reaction. The details are shown below.

4.1 Propylene Glycol Conversion

All structures of propylene glycol conversion in pinacol rearrangement reaction were optimized using DFT at B3LYP/6-31G(d) level of theory. The zero point energies and thermodynamic quantities of activation steps were derived from the frequency calculations at 298.15 K at the same level of theory.

4.1.1 Acid Catalyzed Reaction

Reaction mechanisms of propylene glycol (PG) conversion to propanal (PPNL) and propanone (PPNE) of various acid-catalyzed water-addition models of three concerted pathways are found. The electrostatic potential energies of PG, PPNL and PPNE are shown in Figures 4.1, 4.2 and 4.3, respectively. For molecular electrostatic potential energy of propylene glycol, the positive potentials (blue regions) are located on the hydrogen atoms of OH groups whilst negative potentials (red regions) are located on oxygen atoms. The molecular electrostatic potential energies of propanal and propanone are different from that of propylene glycol in which there are slightly positive potentials because there have not any acidic site.

The propylene glycol conversions have been investigated using the protonated forms of propylene glycol (HPG^+), propanal ($HPPNL^+$) and propanone ($HPPNE^+$). A representative scheme of a whole concerted reaction mechanisms of propylene glycol conversion to propanal and propanone via transition states TS1, TS2 and TS3 which are the secondary and primary carbonium ions is shown in Figure 4.4. Total energies and geometrical structures of species HPG^+, $HPPNL^+$ and $HPPNE^+$ and the corresponding transition states of various acid-catalyzed models are determined at the B3LYP/6-31G(d) level of theory with zero point energy corrections.

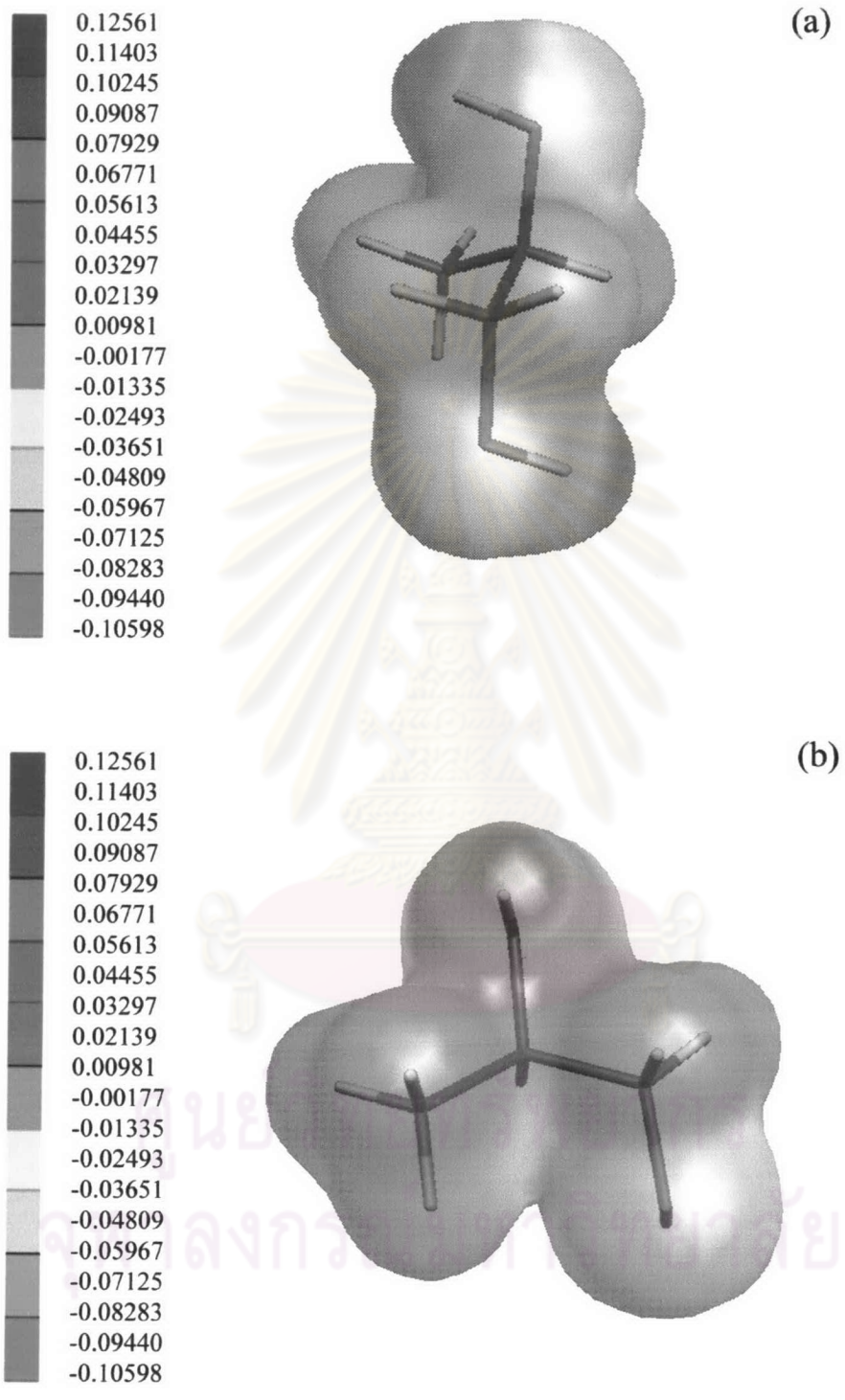

Figure 4.1 Molecular electrostatic potential energy of propylene glycol(PG): (a) side view and (b) front view.

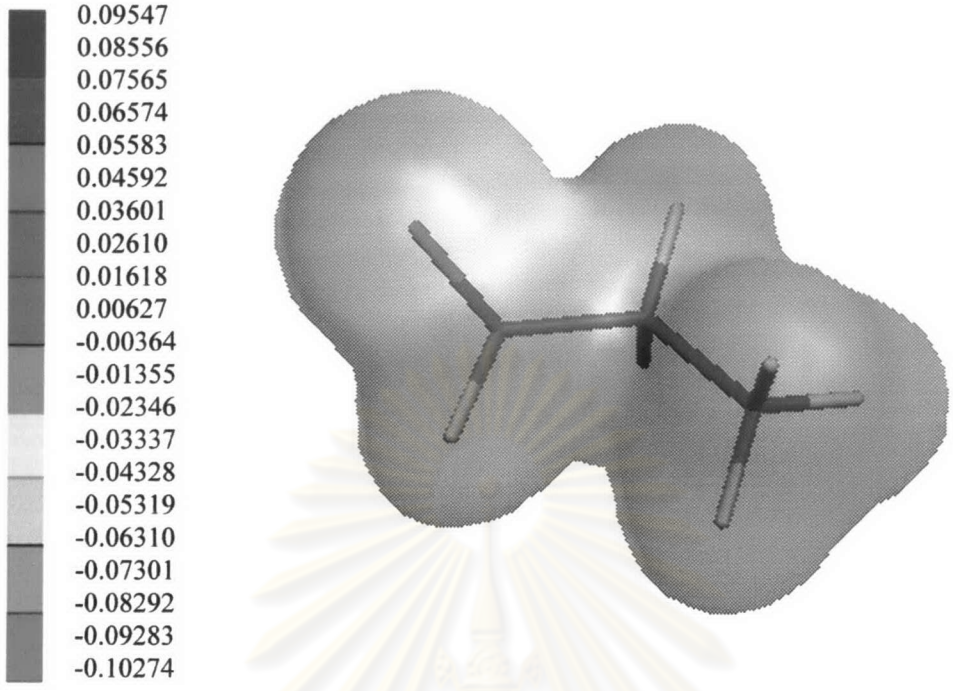

Figure 4.2 Molecular electrostatic potential energy of propanal (PPNL).

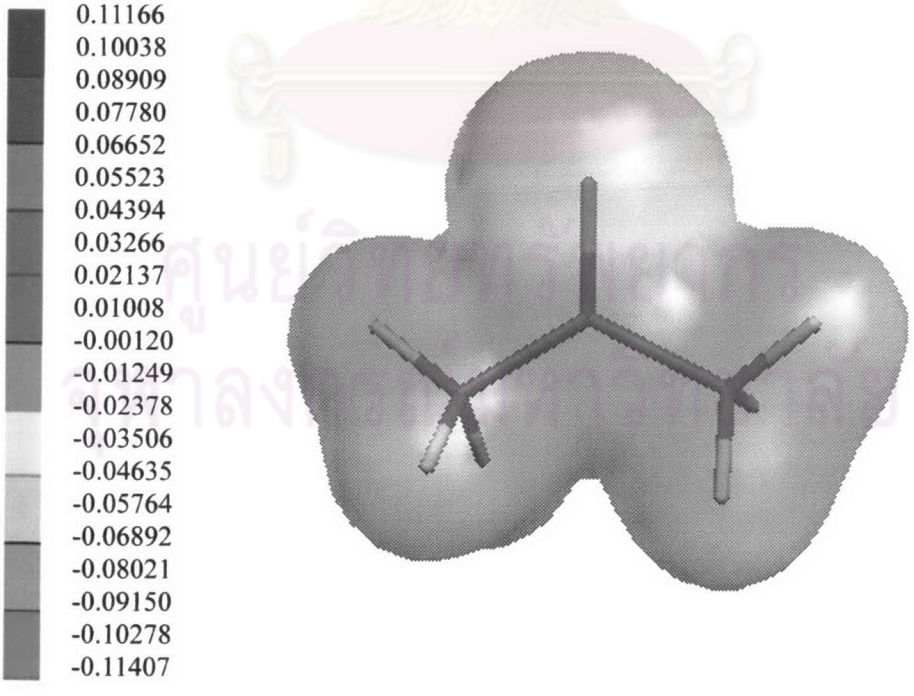

Figure 4.3 Molecular electrostatic potential energy of propanone (PPNE).

There are three concerted pathways in pinacol rearrangement of propylene glycol, C1H, C1Me and C2H. When the water molecule of protonated propylene glycol is lost at carbon 2, the rearrangement can occur in two pathways. One is C1H pathway which means that hydrogen atom is migrated from carbon 1. The other is pathway that methyl group is migrated, C1Me pathway. While carbon 1 of protonated propylene glycol is lost water molecule, there have two equivalent hydrogen atoms from carbon 2 to migrate. Thus, there is only one pathway, C2H pathway, when carbon 1 is dehydration. The three concerted pathways (1) C1H, (2) C1Me and (3) C2H via transition states TS1 and TS2, and TS3 have became the products $HPPNL^+$ and $HPPNE^+$, respectively. Figure 4.4 shows that the product $HPPNL^+$ is produced via transition states TS1 and TS2, whilst $HPPNE^+$ is produced via transition state TS3.

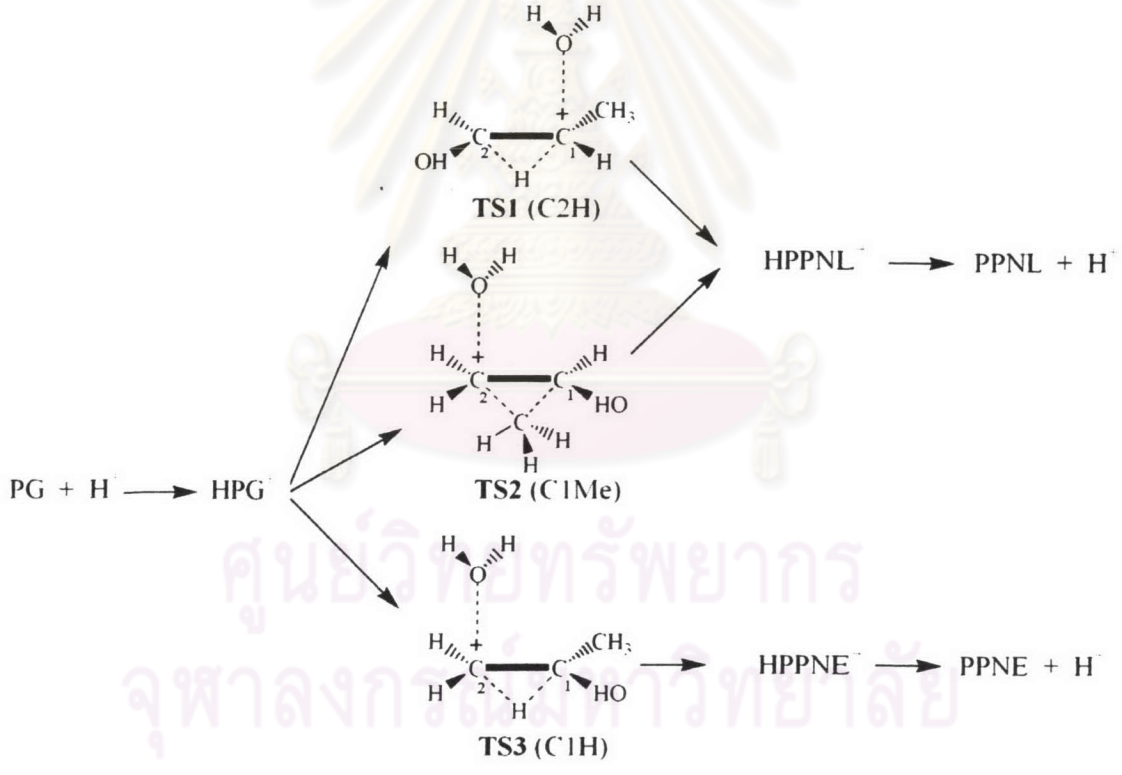

Figure 4.4 A representative scheme of reaction mechanism of propylene glycol in pinacol rearrangement.

In this work, four acid-catalyzed models for the pinacol rearrangement of propylene glycol are studied. The first model, model I, is the gas phase model whilst the other models, model II to model IV, are the aqueous phase models which water molecules are added. Model II is added one water molecule while model III and model IV are added two and three water molecules, respectively. The zero point energies and activation thermodynamic quantities, forward and backward rate constants of acid-catalyzed reaction models I, II, III and IV are shown in Tables 4.1, 4.2, 4.3 and 4.4, respectively. The magnitude orders of forward rate constants of four reaction models as tabulated in Table 4.1 to 4.4 are concluded as

model I: k_1^J (C2H) >> k_3^J (C1H) >> k_2^J (C1Me),

model II: k_1^J (C2H) >> k_3^J (C1H) >> k_2^J (C1Me),

model III: k_1^J (C2H) > k_3^J (C1H) >> k_2^J (C1Me),

model IV: k_3^J (C1H) ~ k_1^J (C2H) >> k_2^J (C1Me).

The typical structures of transition states TS1, TS2 and TS3 are the secondary (C2H), primary (C1Me) and primary (C1H) carbonium cations, respectively. As the decreasing order of structural stability of carbonium ions is as tertiary > secondary > primary, the secondary carbonium ion of transition state TS1 (C2H) is the stable species in gas-phase which is much more stable than the transition states TS2 and TS3 in gas-phase which is defined as model I. As the primary carbonium ions of transition states TS2 (C1Me) and TS3 (C1H) are stabilized in aqueous-phase which is defined as model IV, the tri-hydration of TS3 (C1H) is found to be more stable than its mono-hydration in model I. The stability order of transition state TS3 with respect to TS1 and TS2 is remarkable changed at high number of hydration water of model IV as shown in following scheme.

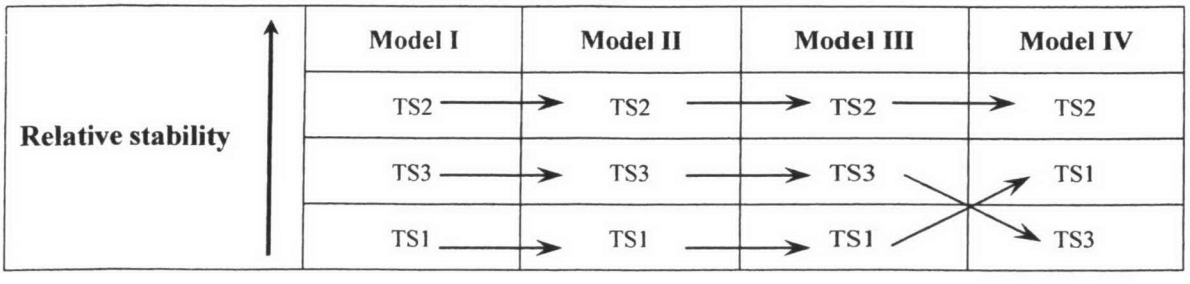

Relative energetic profiles for acid-catalyzed reaction models I, II, III and IV are shown in Figures 4.13 a, b, c and d, respectively. The activation energies of three concerted mechanisms of various acid-catalyzed reaction models computed at B3LYP/6-31G(d) // B3LYP/6-31G(d), B3LYP/6-31G(d, p) // B3LYP/6-31G(d) and B3LYP/6-311G(d) // B3LYP/6-31G(d) levels of theory are tabulated in Table 4.6. From that table, the activation energies derived from the total energies of transition states TS1, TS2 and TS3 using single point calculations are in the same order of magnitudes with respect to the B3LYP/6-31G(d) energies of zero-point energy corrections. The reactant HPG^+, transition states TS1, TS2 and TS3 and products $HPPNL^+$ and $HPPNE^+$ in models I, II, III, IV and V are shown in Figures 4.5, 4.7, 4.9 and 4.11, respectively. Of those figures, the O—H distances of hydrogen bond of intermolecular interaction between water molecules and involved species and their dipole moments are also shown. The energies diagrams of pinacol rearrangement of propylene glycol in models I, II, III, and IV are shown in Figures 4.6, 4.8, 4.10, and 4.12, respectively. The percent compositions of products $HPPNL^+$ and $HPPNE^+$ derived from equation 3.3 are tabulated in Table 4.5. The models I, II and III in Table 4.5 result that the $HPPNL^+$ is the dominant product of which percent is larger than 85 %. For the product ratio of $HPPNL^+$ to $HPPNE^+$ of the model IV is 46.59 to 53.41. These support the acknowledgement that pinacol rearrangements in acid catalyst in aqueous phase are occurred rapidly but the reactions are difficult to control the product selectivity.

The transition states involve in the rearrangement of protonated propylene glycol to $HPPNL^+$ and $HPPNE^+$ product species. The transition state geometries might be related to the reactant and product geometries as per the Hammond's postulate *[51]* which postulates that the transition state geometry of highly exothermic reactions is similar to the reactant, but in highly endothermic reactions the product is a better model for the transition state. For propylene glycol in pinacol rearrangement, it can be observed from the relative energetic profiles that the reaction is slightly exothermic (ΔE ranged from -17.44 to 33.36 kcal/mol). The transition state geometries present that the migration groups of TS1, TS2 and TS3 (proton for TS1 and TS3 and methyl group for TS2) from all models are closer to the structure before migration than the structure of product. Thus, these results are in good accordance with Hammond's postulate.

Table 4.1 Activation thermodynamic quantities and rate constants of acid-catalyzed reaction model I.

Reaction	$\Delta^{\ddagger}E^{O}$,[a]	$\Delta^{\ddagger}H^{O}$,[a]	$\Delta^{\ddagger}G^{O}$,[a]	$\Delta^{\ddagger}S^{O}$,[b]	k,[c]
C2H pathway					
k_1^f : $HPG^+ \longrightarrow$ TS1	18.65	20.19	16.37	12.80	6.21×10^{0}
k_1^b : $HPPNL^+ \longrightarrow$ TS1	36.06	36.45	35.87	1.96	3.16×10^{-14}
C1Me pathway					
k_2^f : $HPG^+ \longrightarrow$ TS2	24.73	25.90	23.17	9.16	6.40×10^{-5}
k_2^b : $HPPNL^+ \longrightarrow$ TS2	42.15	42.17	42.67	-1.68	3.26×10^{-19}
C1H pathway					
k_3^f : $HPG^+ \longrightarrow$ TS3	21.44	22.25	20.36	6.34	7.32×10^{-3}
k_3^b : $HPPNE^+ \longrightarrow$ TS3	53.11	52.56	54.09	-5.12	1.39×10^{-27}

[a] in kcal/mol. [b] in cal/mol K. [c] forward (k^f) and backward (k^b) rate constants.

Table 4.2 Activation thermodynamic quantities and rate constants of acid-catalyzed reaction model II.

Reaction	$\Delta^{\ddagger}E^{O}$,[a]	$\Delta^{\ddagger}H^{O}$,[a]	$\Delta^{\ddagger}G^{O}$,[a]	$\Delta^{\ddagger}S^{O}$,[b]	k,[c]
C2H pathway					
k_1^f : $HPG^+ \longrightarrow$ TS1	26.25	27.58	24.26	11.11	1.01×10^{-5}
k_1^b : $HPPNL^+ \longrightarrow$ TS1	37.01	37.40	37.85	-1.48	1.12×10^{-15}
C1Me pathway					
k_2^f : $HPG^+ \longrightarrow$ TS2	32.51	33.77	30.12	12.25	5.20×10^{-10}
k_2^b : $HPPNL^+ \longrightarrow$ TS2	43.28	43.60	43.70	-0.34	5.76×10^{-20}
C1H pathway					
k_3^f : $HPG^+ \longrightarrow$ TS3	29.13	29.97	27.97	6.72	1.96×10^{-8}
k_3^b : $HPPNE^+ \longrightarrow$ TS3	54.04	53.58	55.64	-6.92	1.01×10^{-28}

[a] in kcal/mol. [b] in cal/mol K. [c] forward (k^f) and backward (k^b) rate constants.

Table 4.3 Activation thermodynamic quantities and rate constants of acid-catalyzed reaction model III.

Reaction		$\Delta^{\ddagger}E^{O}$,[a]	$\Delta^{\ddagger}H^{O}$,[a]	$\Delta^{\ddagger}G^{O}$,[a]	$\Delta^{\ddagger}S^{O}$,[b]	k,[c]
C2H pathway						
k_1^f : HPG$^+$	⟶ TS1	28..80	29.91	26.79	10.45	1.42 x 10^{-7}
k_1^b : HPPNL$^+$	⟶ TS1	46.14	46.21	46.93	-2.42	2.45 x 10^{-22}
C1Me pathway						
k_2^f : HPG$^+$	⟶ TS2	34.89	36.17	32.38	12.71	1.14 x 10^{-11}
k_2^b : HPPNL$^+$	⟶ TS2	52.23	52.46	52.52	-0.17	1.97 x 10^{-26}
C1H pathway						
k_3^f : HPG$^+$	⟶ TS3	29.28	29.94	28.03	6.39	1.75 x 10^{-8}
k_3^b : HPPNE$^+$	⟶ TS3	55.61	55.20	56.58	-4.63	2.08 x 10^{-29}

[a] in kcal/mol. [b] in cal/mol K. [c] forward (k^f) and backward (k^b) rate constants.

Table 4.4 Activation thermodynamic quantities and rate constants of acid-catalyzed reaction model IV.

Reaction		$\Delta^{\ddagger}E^{O}$,[a]	$\Delta^{\ddagger}H^{O}$,[a]	$\Delta^{\ddagger}G^{O}$,[a]	$\Delta^{\ddagger}S^{O}$,[b]	k,[c]
C2H pathway						
k_1^f : HPG$^+$	⟶ TS1	24.45	26.45	21.07	18.05	2.23 x 10^{-3}
k_1^b : HPPNL$^+$	⟶ TS1	47.63	48.09	49.06	-3.27	6.71 x 10^{-24}
C1Me pathway						
k_2^f : HPG$^+$	⟶ TS2	30.51	32.37	27.25	17.17	6.51 x 10^{8}
k_2^b : HPPNL$^+$	⟶ TS2	23.68	54.01	55.25	-4.14	1.96 x 10^{-28}
C1H pathway						
k_3^f : HPG$^+$	⟶ TS3	23.71	25.27	20.99	14.37	2.56 x 10^{-3}
k_3^b : HPPNE$^+$	⟶ TS3	57.06	56.87	59.47	-8.71	1.58 x 10^{-31}

[a] in kcal/mol. [b] in cal/mol K. [c] forward (k^f) and backward (k^b) rate constants.

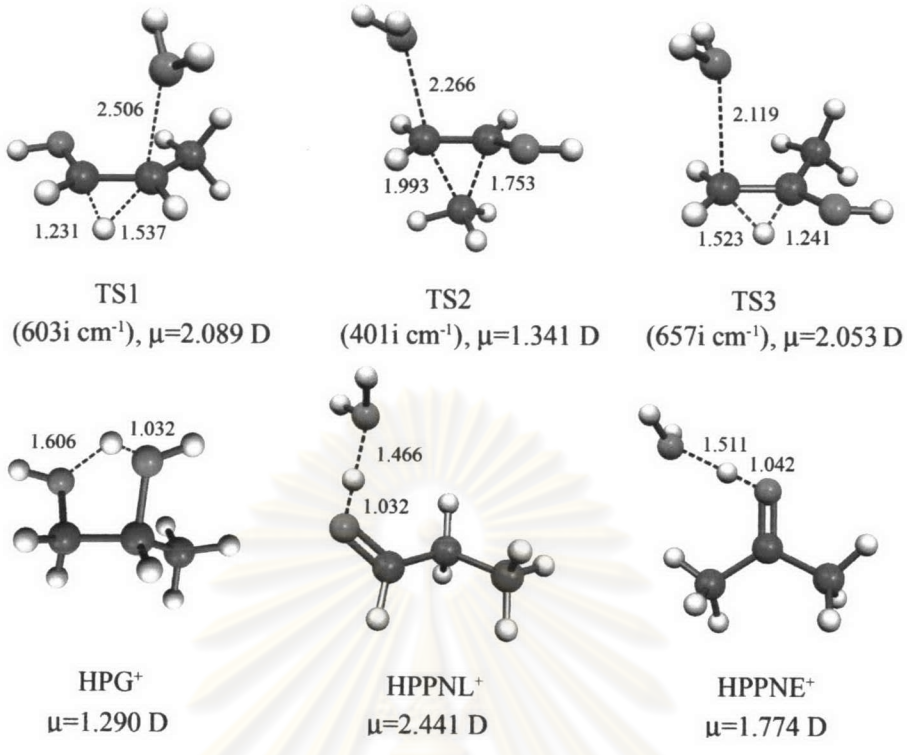

Figure 4.5 The B3LYP/6-31G(d) optimized geometries of conversion reaction mode I of transition states, reactant and two products. Hydrogen bond distances are in angstroms and dipole moments are reported. The imaginary frequencies of transition states are in parentheses.

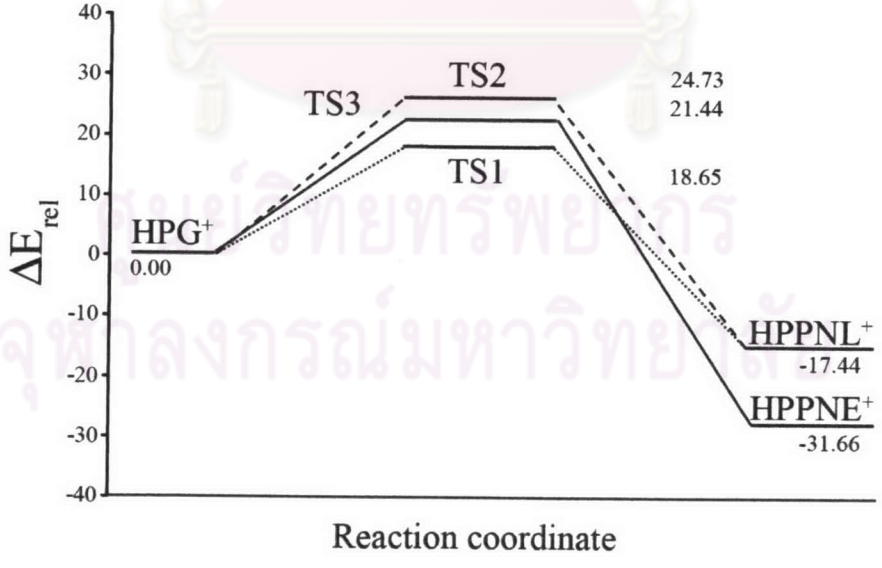

Figure 4.6 Relative energetic profiles of conversion reactions of model I. All energies (in kcal/mol) are based upon total energies with respect to reactant HPG^+ computed at B3LYP/6-31G(d) level of theory.

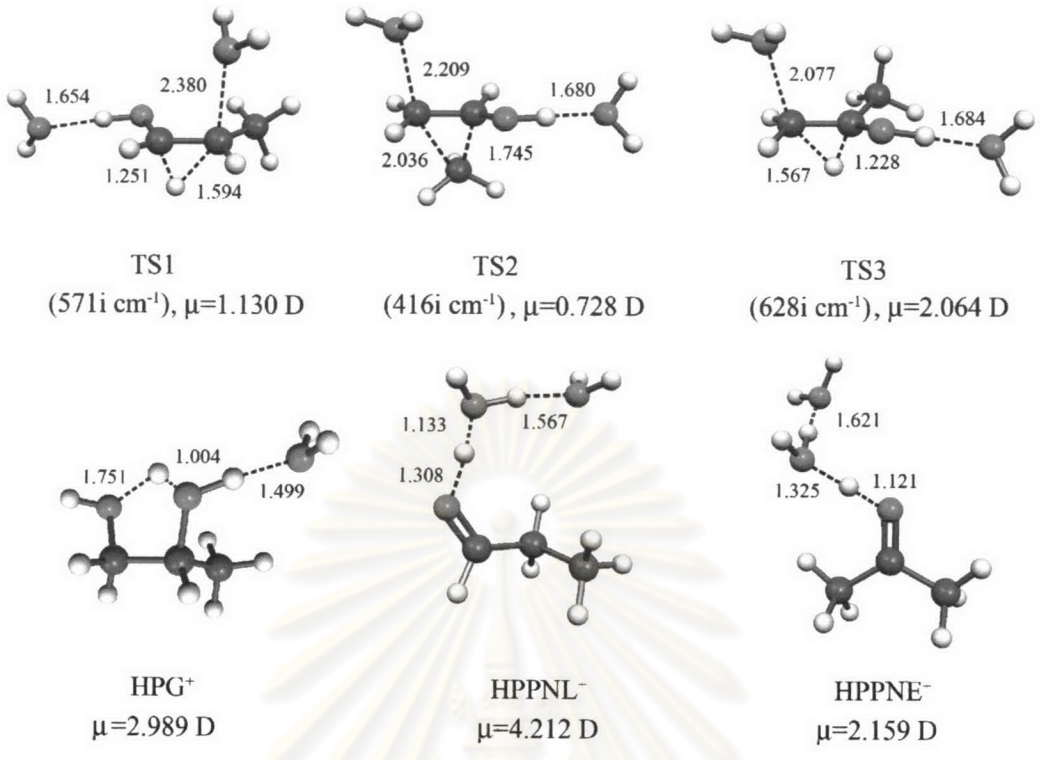

Figure 4.7 The B3LYP/6-31G(d) optimized geometries of conversion reaction model II of transition states, reactant and two products.

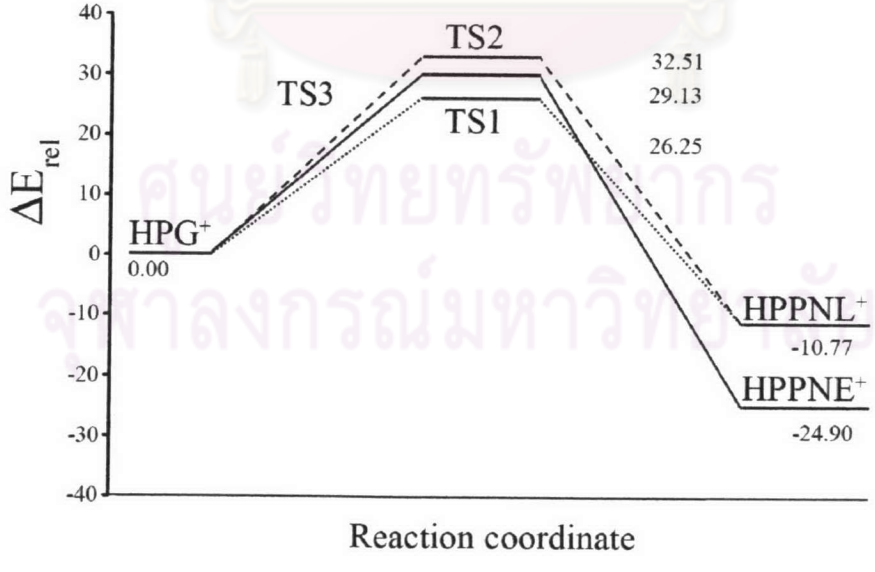

Figure 4.8 Relative energetic profiles of conversion reactions of model II.

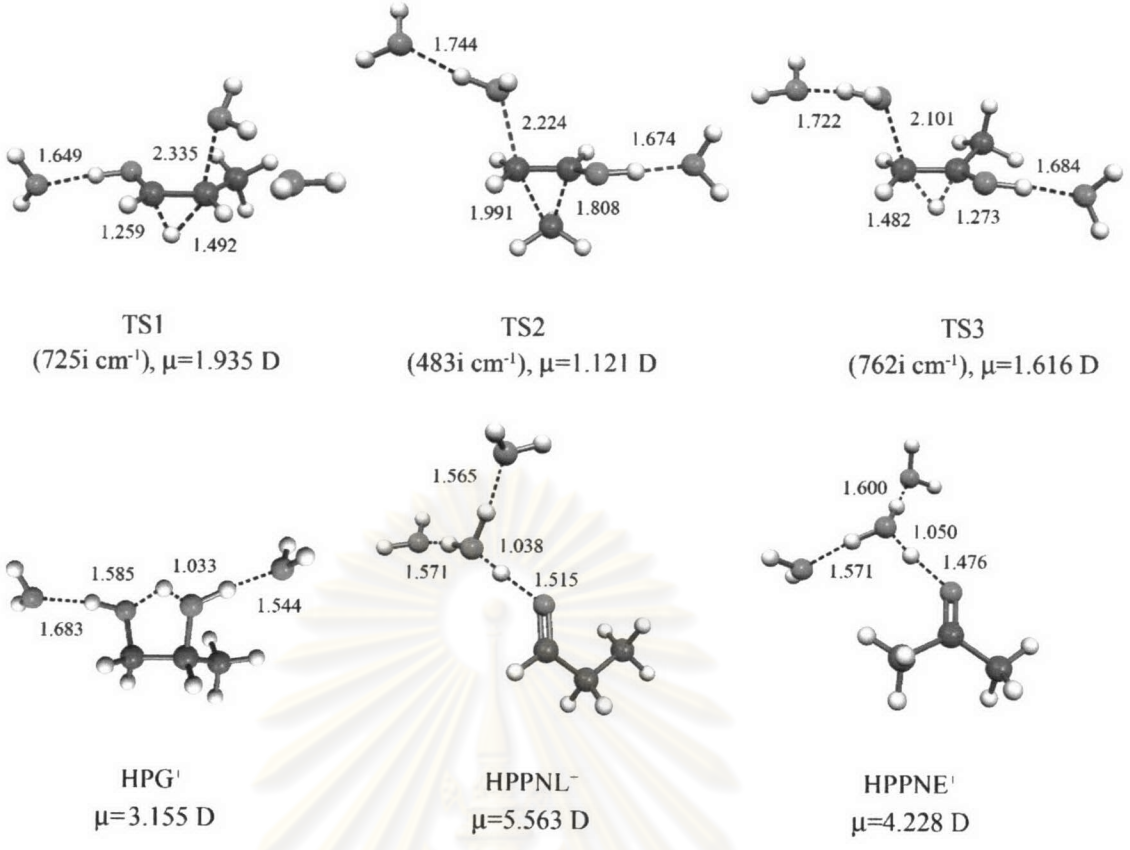

Figure 4.9 The B3LYP/6-31G(d) optimized geometries of conversion reaction model III of transition states, reactant and two products.

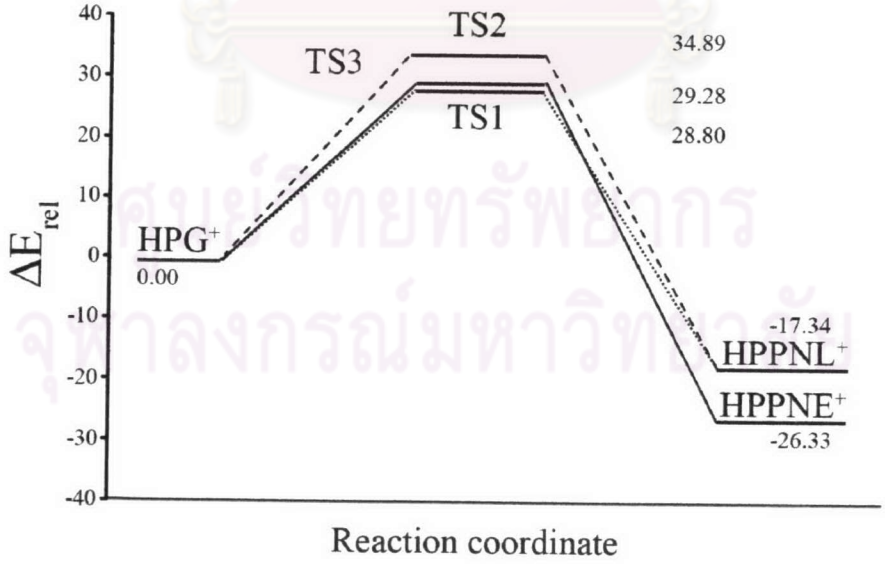

Figure 4.10 Relative energetic profiles of conversion reactions of model III.

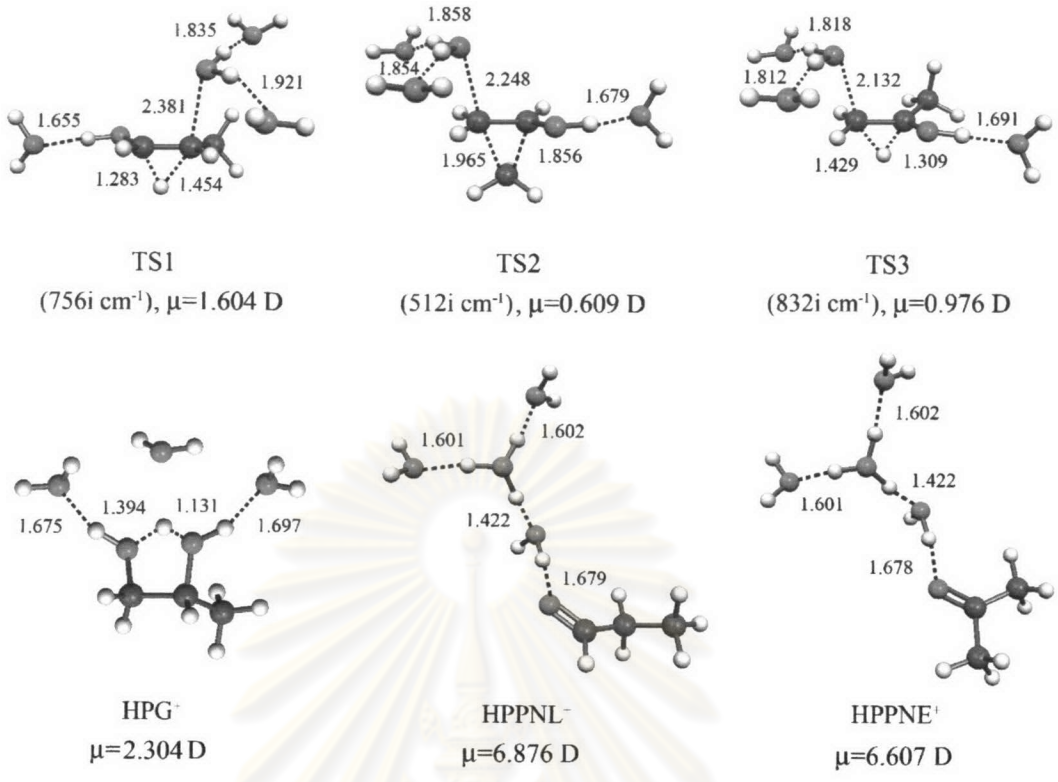

Figure 4.11 The B3LYP/6-31G(d) optimized geometries of conversion reaction model IV of transition states, reactant and two products.

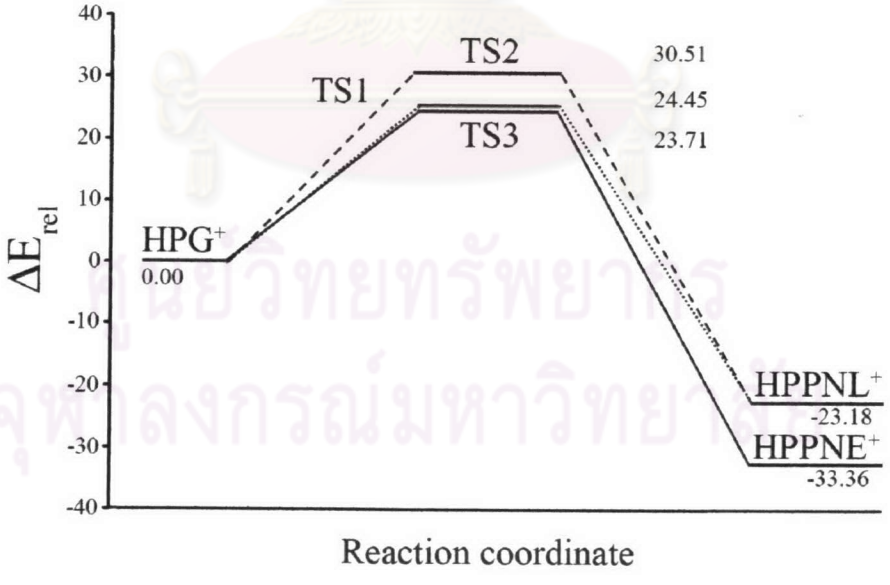

Figure 4.12 Relative energetic profiles of conversion reactions of model IV.

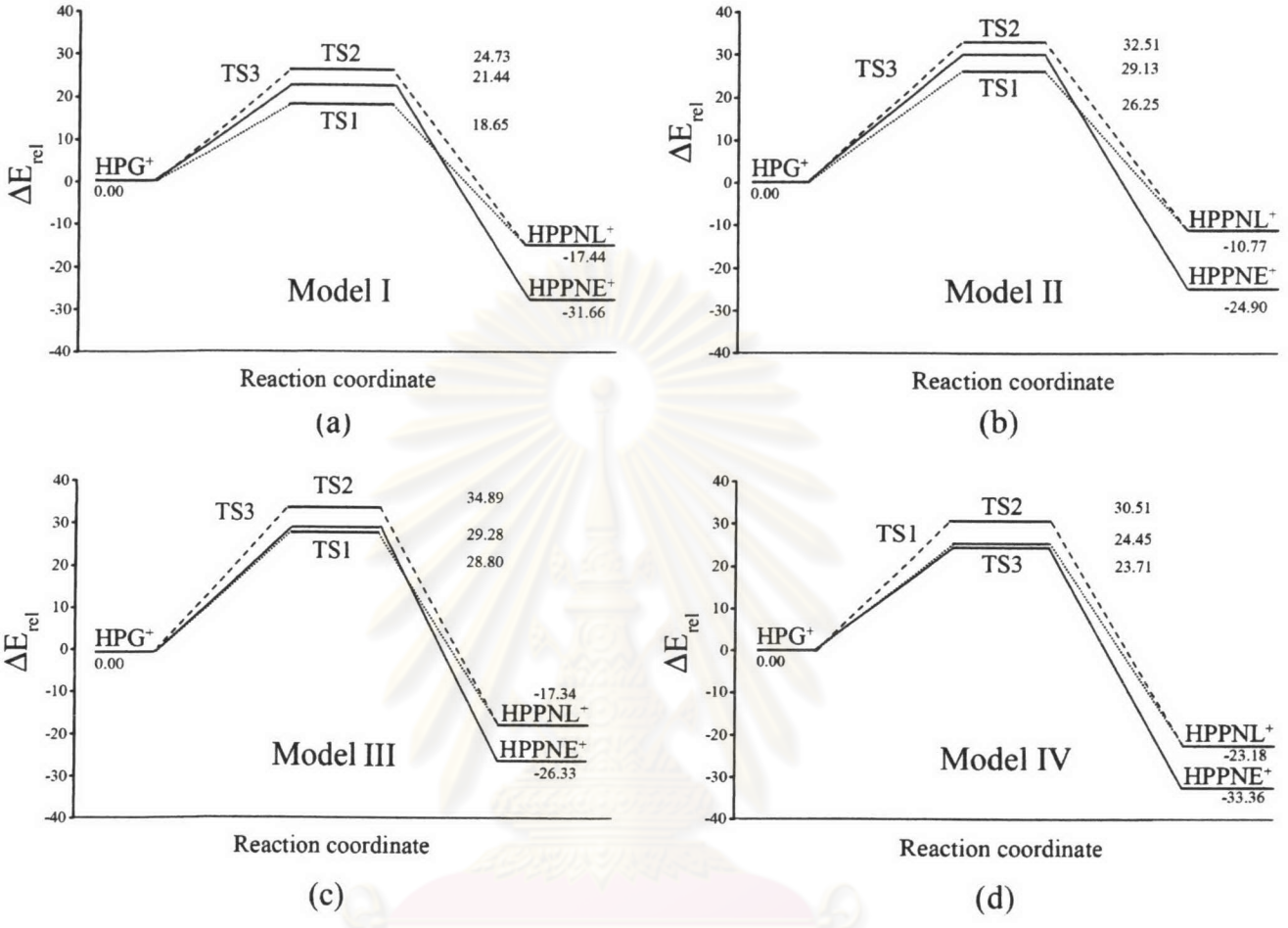

Figure 4.13 Relative energetic profiles of conversion reactions of (a) model I, (b) model II, (c) model III and (d) model IV. All energies (in kcal/mol) are based upon total energies with respect to reactant HPG^+ computed at B3LYP/6-31G(d) level of theory with zero-point energy corrections.

Table 4.5 Percent of product compositions of $HPPNL^+$ and $HPPNE^+$ and its ratio based upon the B3LYP/6-31G(d) computation.

Model	$[HPPNL^+]$ [a]	$[HPPNE^+]$ [a]	$[HPPNL^+]:[HPPNE^+]$ [b]
I.	99.88	0.12	848.13
II.	99.81	0.19	516.65
III.	89.01	10.99	8.10
IV.	46.59	53.41	0.87

[a] in percent. [b] Computed using equation 3.3.

Table 4.6 Activation energies of the conversion reaction of various acid-catalyzed models computed at various DFT methods.

Transition structure	ΔE_{rel}^{O}, [a]				
	B3LYP/6-31G(d)// B3LYP/6-31G(d) [b]	B3LYP/6-31G(d)// B3LYP/6-31G(d) [c]	B3LYP/6-31G(d)// B3LYP/6-31G(d)	B3LYP/6-31G(d,p) // B3LYP/6-31G(d)	B3LYP/6311G(d,p) // B3LYP/6-31G(d)
Model I					
TS1	18.65	18.28	24.20	23.14	19.76
TS2	24.73	24.25	28.53	28.20	25.68
TS3	21.44	21.02	25.78	24.90	22.51
Model II					
TS1	26.25	25.73	30.84	30.20	26.93
TS2	32.51	31.88	36.21	36.32	33.67
TS3	29.13	28.56	33.32	32.86	30.36
Model III					
TS1	28.80	28.23	33.23	32.54	28.99
TS2	34.89	34.21	38.38	38.48	35.31
TS3	29.28	28.71	33.11	32.59	29.76
Model IV					
TS1	24.45	23.97	27.32	26.29	21.94
TS2	30.51	29.91	31.74	31.59	27.85
TS3	23.71	23.24	25.89	25.12	21.59

[a] in kcal/mol. [b] with ZPE corrections. [c] with ZPE corrections, scaled by 0.9804.

4.1.2 Zeolite HZSM-5 Catalyst

The structure of zeolite HZSM-5 used in this study are 3T and 5T cluster models. All structures are optimized using DFT at B3LYP/6-31G(d) level of theory. The optimized structures of 3T and 5T are shown in Figure 4.14. Three dimensional surfaces of electrostatic potential of 3T and 5T cluster models are shown in Figure 4.15. The lowest electrostatic potential (red region) is in the proximity of the lone pair of the oxygen atom, whereas the positive potential (blue region) is in hydrogen atom which represented zeolite proton. The result form electrostatic potential corresponds to the acidity of zeolite proton. The results from both 3T and 5T cluster models give the same attitude.

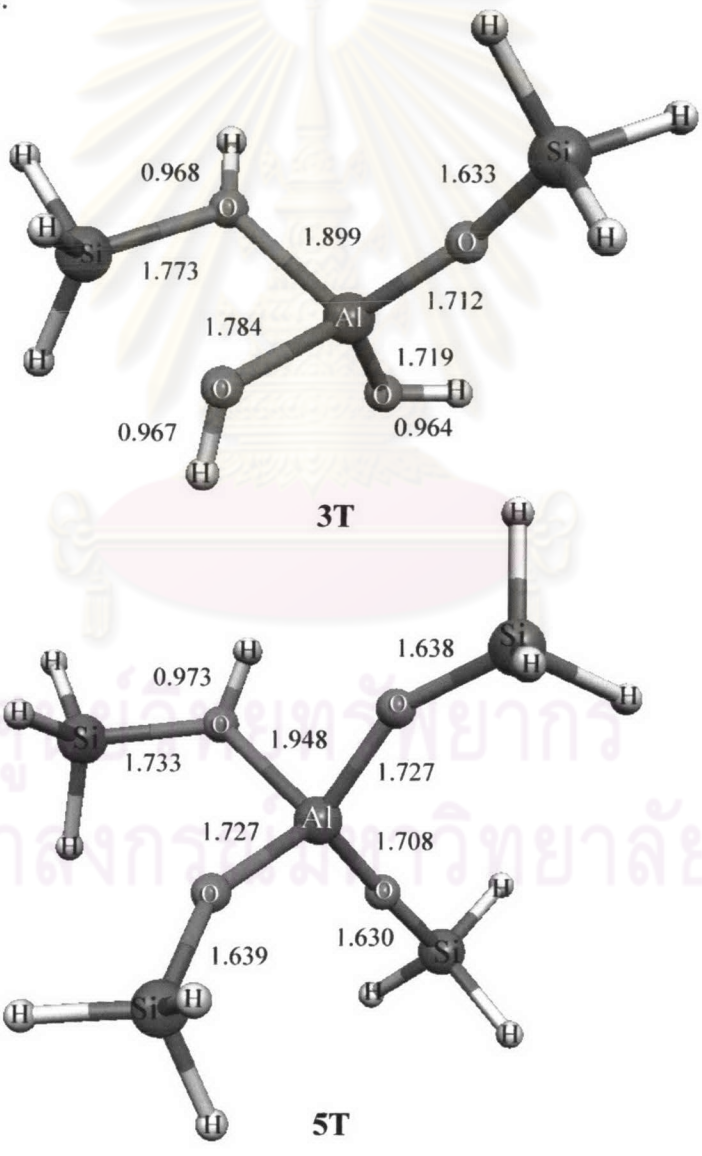

Figure 4.14 Structural geometries of 3T and 5T cluster models. Bond distances are in angstroms.

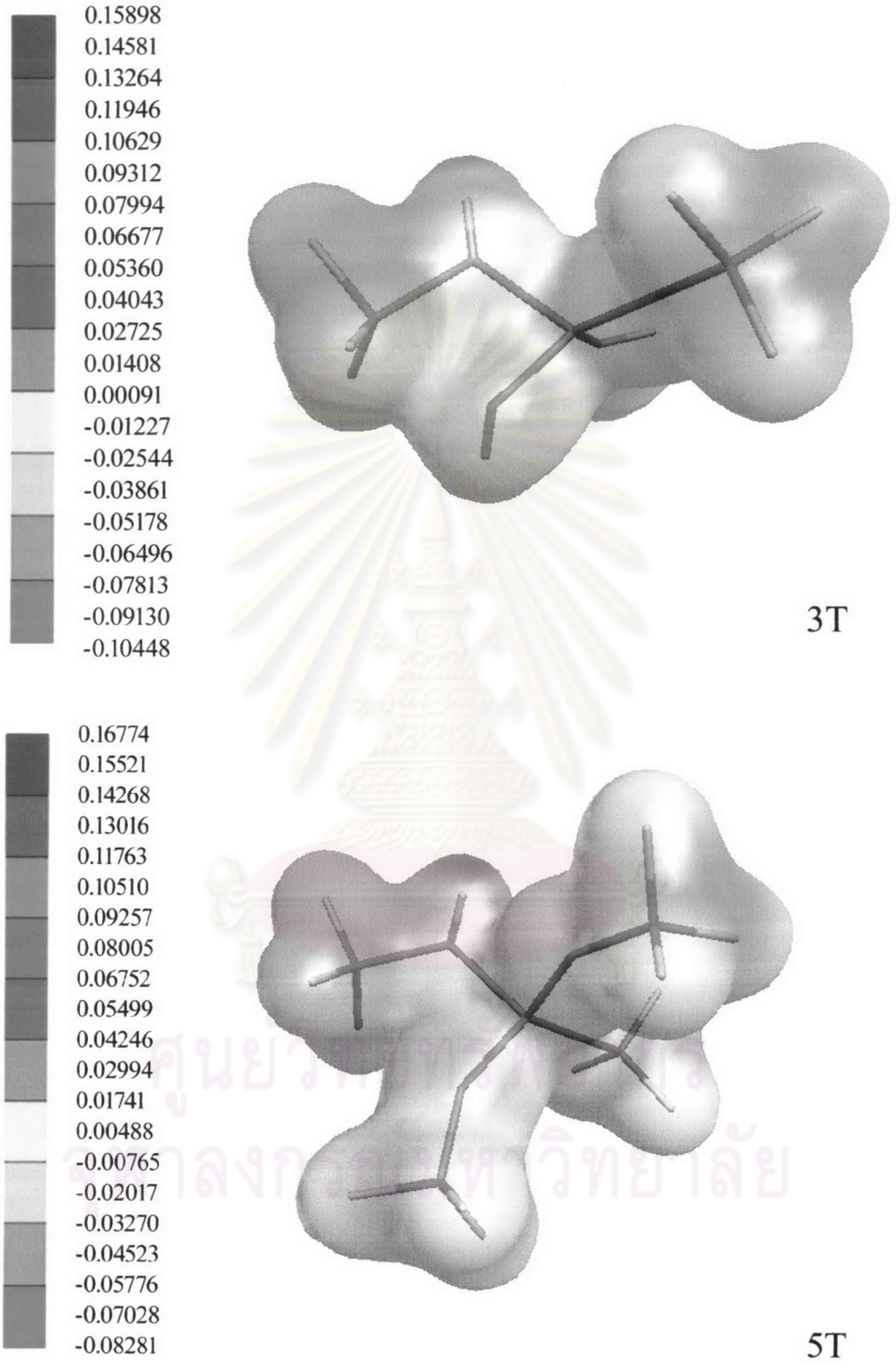

Figure 4.15 Molecular electrostatic potential energies of 3T and 5T cluster models.

The pinacol rearrangements of propylene glycol conversion to propanal and propanone in the zeolite are composed of three reaction path ways namely via the TS1 (C2H), TS2 (C1ME) and TS3 (C1H), as the same as acid catalyst. Two adsorption complexes between the propylene glycol and zeolite were obtained. Complex 1 and complex 2 are the complexes of α and β-hydroxyl oxygen molecules of propylene glycol directly interacting with acid proton of zeolite, respectively. The overall optimized geometries of pinacol rearrangement of propylene glycol over 3T and 5T cluster models are shown in Figures 4.16 and 4.20, respectively.

Geometry parameters of reaction over 3T cluster model in C2H, C1Me and C1Me reaction pathways are shown in Tables 4.7, 4.8 and 4.9, respectively and structural geometries of transition state in C2H, C1Me and C1H reaction pathways are shown in Figures 4.17, 4.18 and 4.9, respectively. Those of reaction over 5T cluster model are shown in Tables 4.10 to 4.12 and Figures 4.21 to 4.23. The zero point energies and activation thermodynamic quantities, forward and backward rate constants of 3T and 5T cluster models are presented in Table 4.13 which shown that activation energy of transition state of C1H pathway is lower than C1Me and C2H pathways. The orders of activation energy of pinacol rearrangement of propylene glycol in zeolite models are as TS2 (C1Me) > TS1 (C2H) > TS3 (C1H), see details in Figure 4.24.

The percent compositions of PPNL and PPNE products derived from equation 3.3 are tabulated in Table 4.14 which shown that PPNE is the main product of the pinacol rearrangement of propylene glycol in 3T and 5T models, 97.64 % and 97.43 %, respectively. These results are contrasted with the results from the same reaction in acid catalyst in aqueous phase which show that PPNL is the main product. According to the results from model IV of acid catalyst in aqueous phase which included three water molecules assisted in model, the percent ratio of product compositions of PPNL and PPNE are 46.59% and 53.41%, respectively. It can be observed that although activation energies of pinacol rearrangement of propylene glycol in acid catalyst and zeolite are in the same range (30-40 kcal/mol) but the selectivity of reaction in zeolite is higher than those of acid catalyst in aqueous phase.

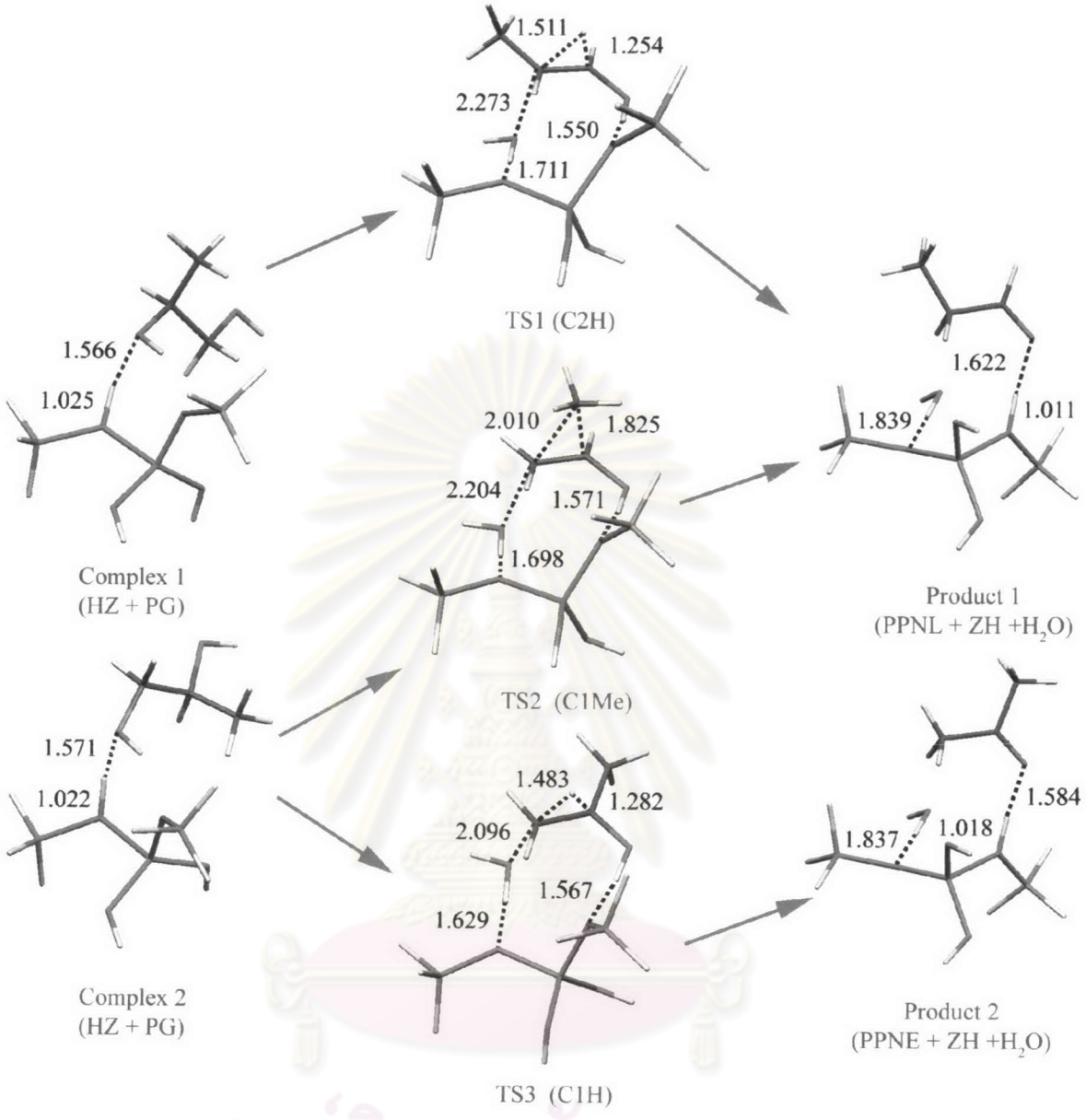

Figure 4.16 The overall optimized geometries of pinacol rearrangement of propylene glycol reaction in 3T cluster model. Bond distances are in angstroms.

Table 4.7 Selected geometrical parameters (bond distances and bond angles) of C2H pathway on 3T cluster model in pinacol rearrangement of propylene glycol

System/parameter	Reaction state			
	HZ	Complex 1	TS1	Product 1
C2H				
r (C_1 - C_2) [a]	-	1.5301	1.4198	1.4999
r (C_1 - O_1) [a]	-	1.4474	2.2731	-
r (C_2 - O_2) [a]	-	1.4203	1.3230	1.2251
r (O'_1 - H') [a]	0.9677	1.0304	1.7109	1.8389
r (O'_2 - H_2) [a]	-	-	1.5498	1.0108
r (O_1 - H_1) [a]	-	0.9880	0.9700	0.9687
r (O_1 - H') [a]	-	1.5459	0.9967	0.9821
r (O_2 - H_2) [a]	-	0.9689	1.0274	1.6220
r (Al - O'_1) [a]	1.8993	1.8996	1.8016	1.7608
r (Al - O'_2) [a]	1.7120	1.7634	1.8178	1.8915
α (Si_1 - O'_1 - Al) [b]	110.437	125.397	127.061	136.666
α (Si_2 - O'_2 - Al) [b]	162.754	135.777	124.666	123.822

[a] Bond distance, in angstroms. [b] Angle, in degrees.

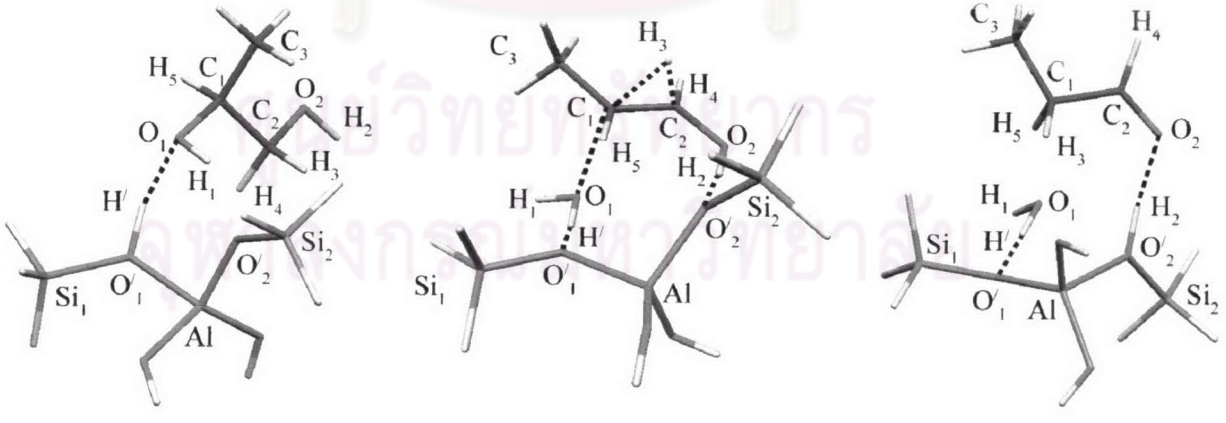

Complex 1 **TS1 (C2H)** **Product 1 (PPNL)**

Figure 4.17 The structural geometries of C2H reaction pathway on 3T cluster model.

Table 4.8 Selected geometrical parameters (bond distances and bond angles) of C1Me pathway on 3T cluster model in pinacol rearrangement of propylene glycol

System/parameter	Reaction state			
	HZ	Complex 2	TS2	Product 1
C1Me				
r (C_1 - C_2) [a]	-	1.5321	1.4090	1.4999
r (C_1 - O_1) [a]	-	1.4284	1.3254	1.2251
r (C_2 - O_2) [a]	-	1.4329	2.2042	-
r (O'_1 - H') [a]	0.9677	1.0219	1.6982	1.8389
r (O'_2 - H_1) [a]	-	-	1.5711	1.0108
r (O_1 - H_1) [a]	-	0.9694	1.0220	1.6220
r (O_2 - H_2) [a]	-	0.9867	0.9710	0.9687
r (O_2 - H') [a]	-	1.5713	0.9996	0.9821
r (Al - O'_1) [a]	1.8993	1.9060	1.8015	1.7608
r (Al - O'_2) [a]	1.7120	1.7680	1.8175	1.8915
α (Si_1 - O'_1 - Al) [b]	110.437	122.208	126.449	136.666
α (Si_2 - O'_2 - Al) [b]	162.754	133.151	124.311	123.822

[a] Bond distance, in angstroms. [b] Angle, in degrees.

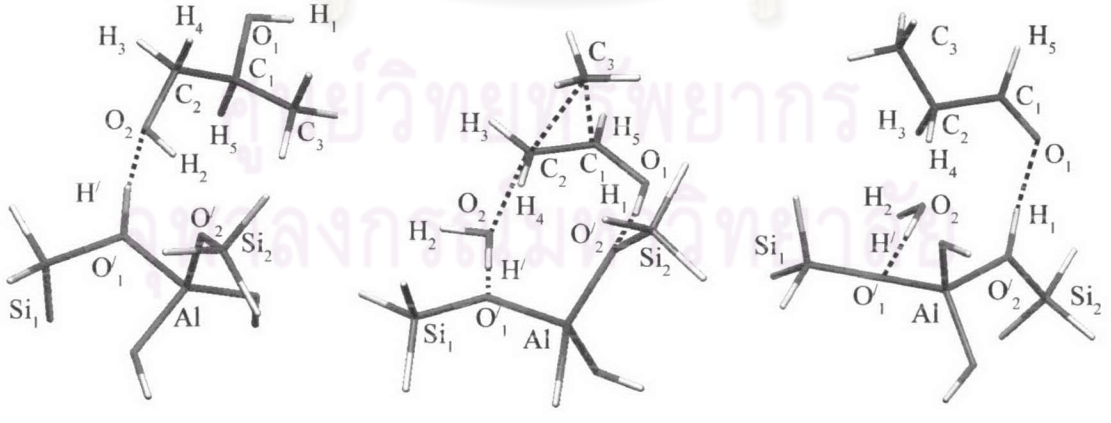

Complex 2 **TS2 (C1Me)** **Product 1 (PPNL)**

Figure 4.18 The structural geometries of C1Me reaction pathway on 3T cluster model.

Table 4.9 Selected geometrical parameters (bond distances and bond angles) of C1H pathway on 3T cluster model in pinacol rearrangement of propylene glycol

System/parameter	Reaction state			
	HZ	Complex 2	TS3	Product 2
C1H				
r (C_1 - C_2) [a]	-	1.5321	1.4235	1.5045
r (C_1 - O_1) [a]	-	1.4284	1.3294	1.2320
r (C_2 - O_2) [a]	-	1.4329	2.0967	3.3583
r (O'_1 - H') [a]	0.9677	1.0219	1.6295	1.8372
r (O'_2 - H_1) [a]	-	-	1.5678	1.0182
r (O_1 - H_1) [a]	-	0.9694	1.0226	1.5845
r (O_2 - H_2) [a]	-	0.9867	0.9716	0.9687
r (O_2 - H') [a]	-	1.5713	1.0102	0.9825
r (Al - O'_1) [a]	1.8993	1.9060	1.8045	1.7619
r (Al - O'_2) [a]	1.7120	1.7680	1.8157	1.8890
α (Si_1 - O'_1 - Al) [b]	110.437	122.208	125.989	136.860
α (Si_2 - O'_2 - Al) [b]	162.754	133.151	125.754	124.494

[a] Bond distance, in angstroms. [b] Angle, in degrees.

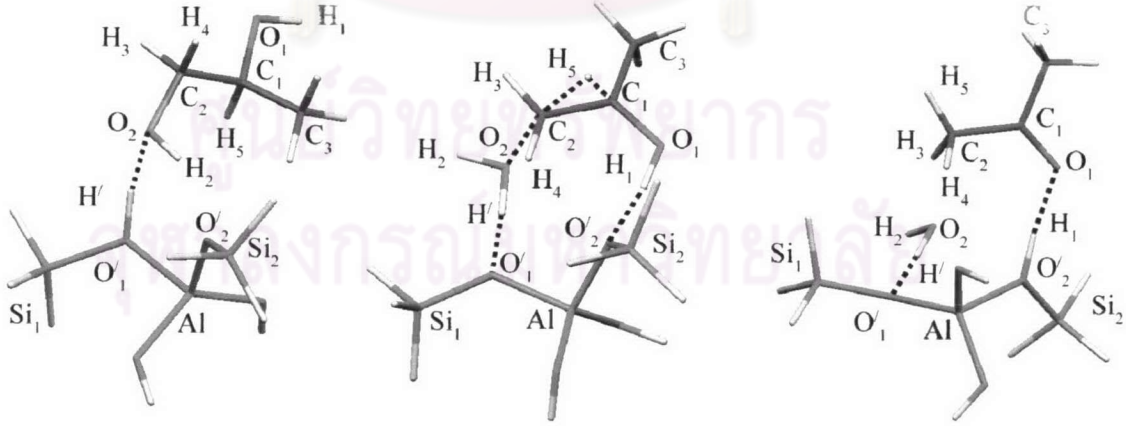

Complex 2 **TS3 (C1H)** **Product 2 (PPNE)**

Figure 4.19 The structural geometries of C1H reaction pathway on 3T cluster model.

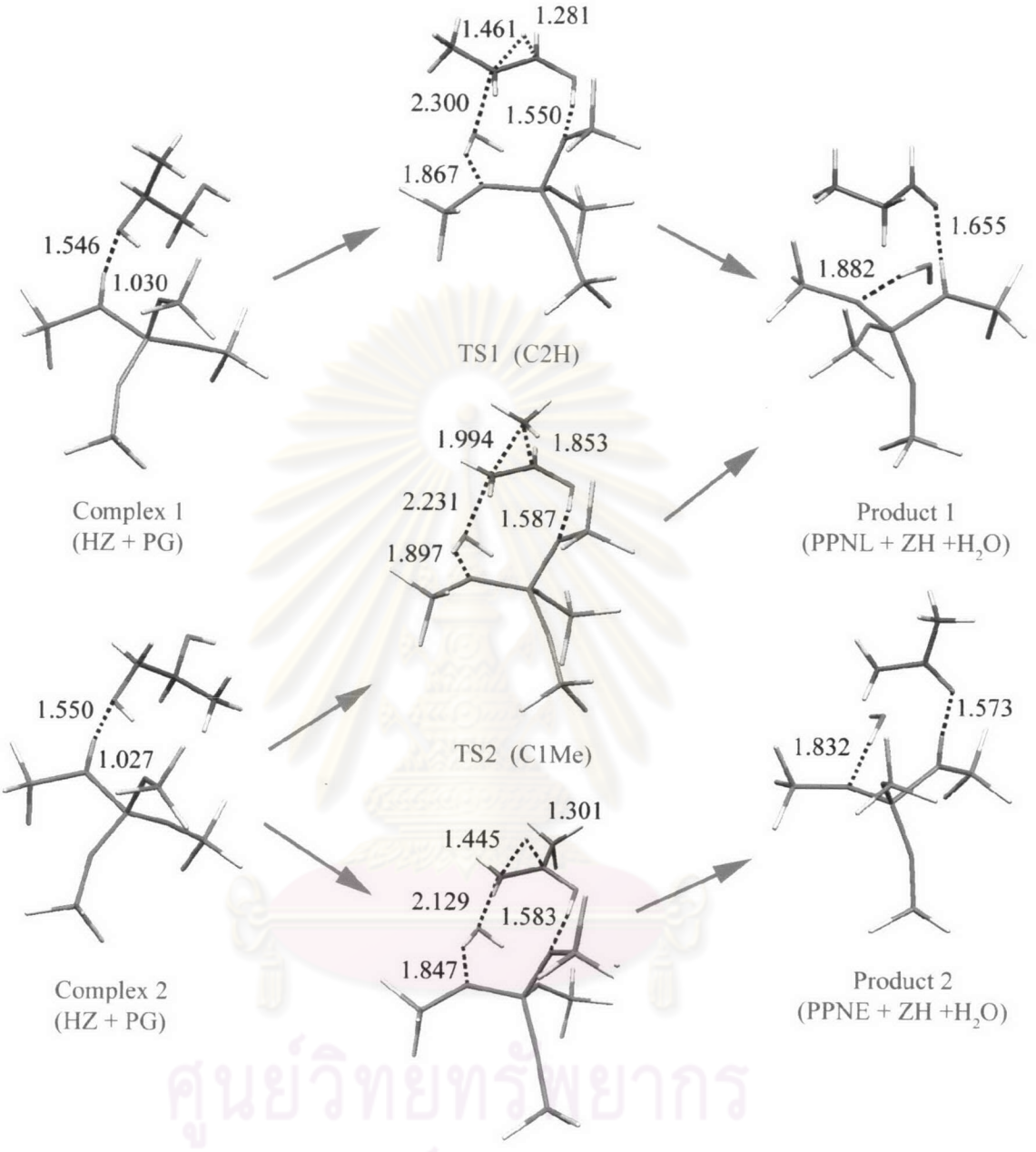

Figure 4.20 The overall optimized geometries of pinacol rearrangement of propylene glycol reaction in 5T cluster model. Bond distances are in angstroms.

Table 4.10 Selected geometrical parameters (bond distances and bond angles) of C2H pathway on 5T cluster model in pinacol rearrangement of propylene glycol

System/parameter	Reaction state			
	HZ	Complex 1	TS1	Product 1
C2H				
r (C_1 - C_2) [a]	-	1.5301	1.4181	1.4995
r (C_1 - O_1) [a]	-	1.4474	2.3115	-
r (C_2 - O_2) [a]	-	1.4203	1.3184	1.2329
r (O'_1 - H') [a]	0.9735	1.0304	1.8674	1.8823
r (O'_2 - H_2) [a]	-	-	1.5501	1.0053
r (O_1 - H_1) [a]	-	0.9880	0.9843	0.9688
r (O_1 - H') [a]	-	1.5459	0.9855	0.9800
r (O_2 - H_2) [a]	-	0.9689	1.0279	1.6549
r (Al - O'_1) [a]	1.9478	1.8996	1.7774	1.7537
r (Al - O'_2) [a]	1.7274	1.7634	1.8086	1.8867
α (Si_1 - O'_1 - Al) [b]	123.283	125.397	135.179	139.009
α (Si_2 - O'_2 - Al) [b]	153.142	135.777	128.534	126.331

[a] Bond distance, in angstroms. [b] Angle, in degrees.

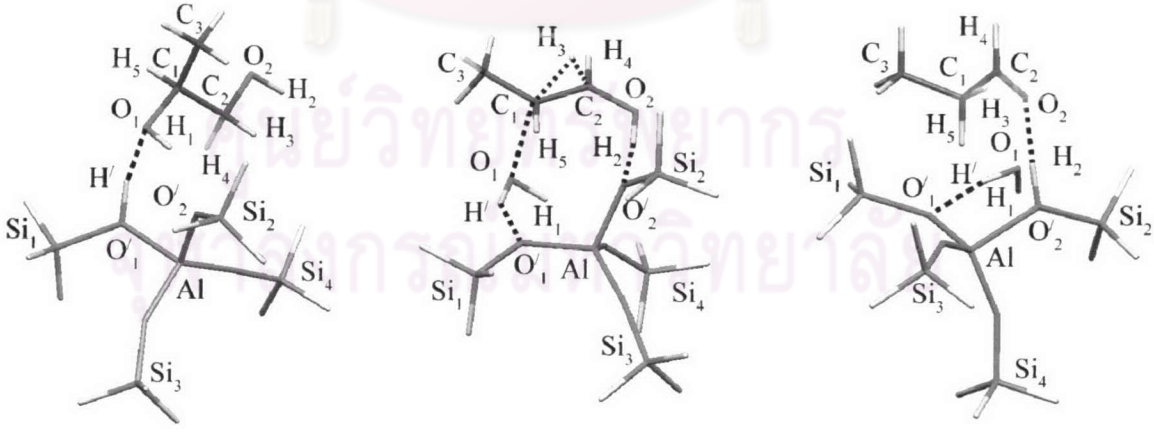

Complex 1 **TS1 (C2H)** **Product 1 (PPNL)**

Figure 4.21 The structural geometries of C2H reaction pathway on 5T cluster model.

Table 4.11 Selected geometrical parameters (bond distances and bond angles) of C1Me pathway on 5T cluster model in the pinacol rearrangement of propylene glycol

System/parameter	Reaction state			
	HZ	Complex 2	TS2	Product 1
C1Me				
r (C_1 - C_2) [a]	-	1.5321	1.4072	1.4995
r (C_1 - O_1) [a]	-	1.4272	1.3229	1.2329
r (C_2 - O_2) [a]	-	1.4347	2.2323	-
r (O'_1 - H') [a]	0.9735	1.0270	1.8977	1.8823
r (O'_2 - H_1) [a]	-	-	1.5871	1.0053
r (O_1 - H_1) [a]	-	0.9695	1.0198	1.6549
r (O_2 - H_2) [a]	-	0.9857	0.9859	0.9688
r (O_2 - H') [a]	-	1.5505	0.9844	0.9800
r (Al - O'_1) [a]	1.9478	1.9007	1.7783	1.7537
r (Al - O'_2) [a]	1.7274	1.7649	1.8073	1.8867
α (Si_1 - O'_1 - Al) [b]	123.283	125.199	134.633	139.009
α (Si_2 - O'_2 - Al) [b]	153.142	135.074	128.818	126.331

[a] Bond distance, in angstroms. [b] Angle, in degrees.

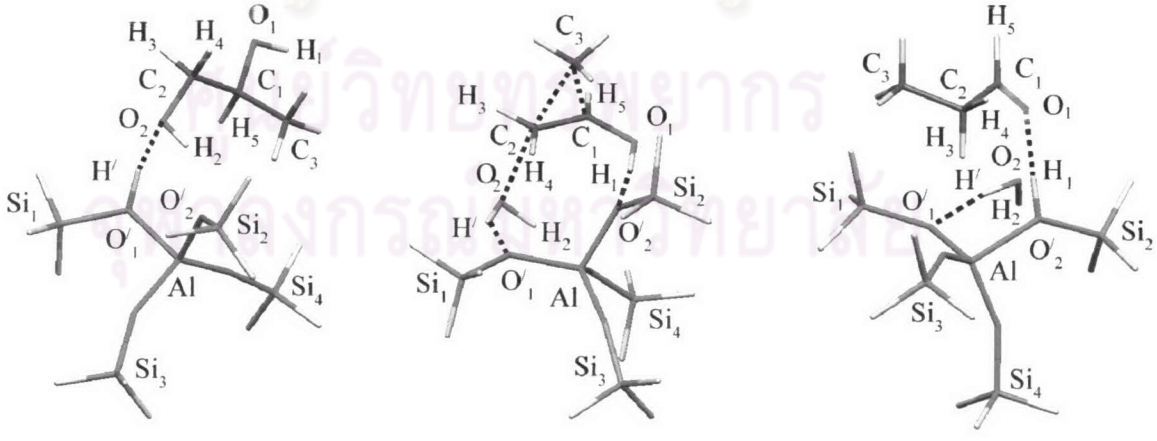

Complex 2 **TS2 (C1Me)** **Product 1 (PPNL)**

Figure 4.22 The structural geometries of C1Me reaction pathway on 5T cluster model.

Table 4.12 Selected geometrical parameters (bond distances and bond angles) of C1H pathway on 5T cluster model in pinacol rearrangement of propylene glycol

System/parameter	Reaction state			
	HZ	Complex 2	TS3	Product 2
C1H				
r (C_1 - C_2) [a]	-	1.5321	1.4227	1.5057
r (C_1 - O_1) [a]	-	1.4272	1.3277	1.2328
r (C_2 - O_2) [a]	-	1.4347	2.1294	3.3303
r (O'_1 - H') [a]	0.9735	1.0270	1.8273	1.8323
r (O'_2 - H_1) [a]	-	-	1.5827	1.0210
r (O_1 - H_1) [a]	-	0.9695	1.0202	1.7582
r (O_2 - H_2) [a]	-	0.9857	0.9897	0.9689
r (O_2 - H') [a]	-	1.5505	0.9886	0.9833
r (Al - O'_1) [a]	1.9478	1.9007	1.7789	1.5738
r (Al - O'_2) [a]	1.7274	1.7649	1.8073	1.8845
α (Si_1 - O'_1 - Al) [b]	123.283	125.199	134.713	137.683
α (Si_2 - O'_2 - Al) [b]	153.142	135.074	129.342	128.613

[a] Bond distance, in angstroms. [b] Angle, in degrees.

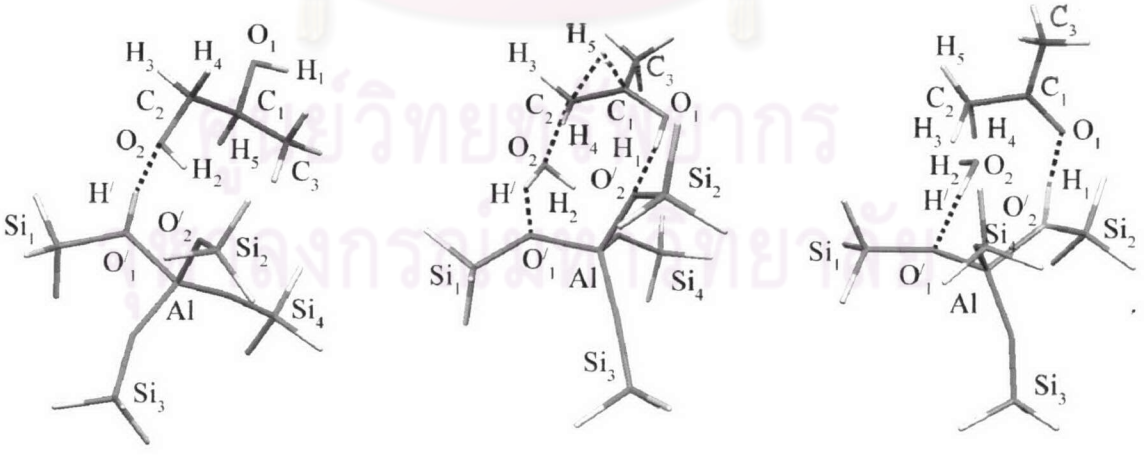

Complex 2 **TS3 (C1H)** **Product 2 (PPNE)**

Figure 4.23 The structural geometries of C1H reaction pathway on 5T cluster model.

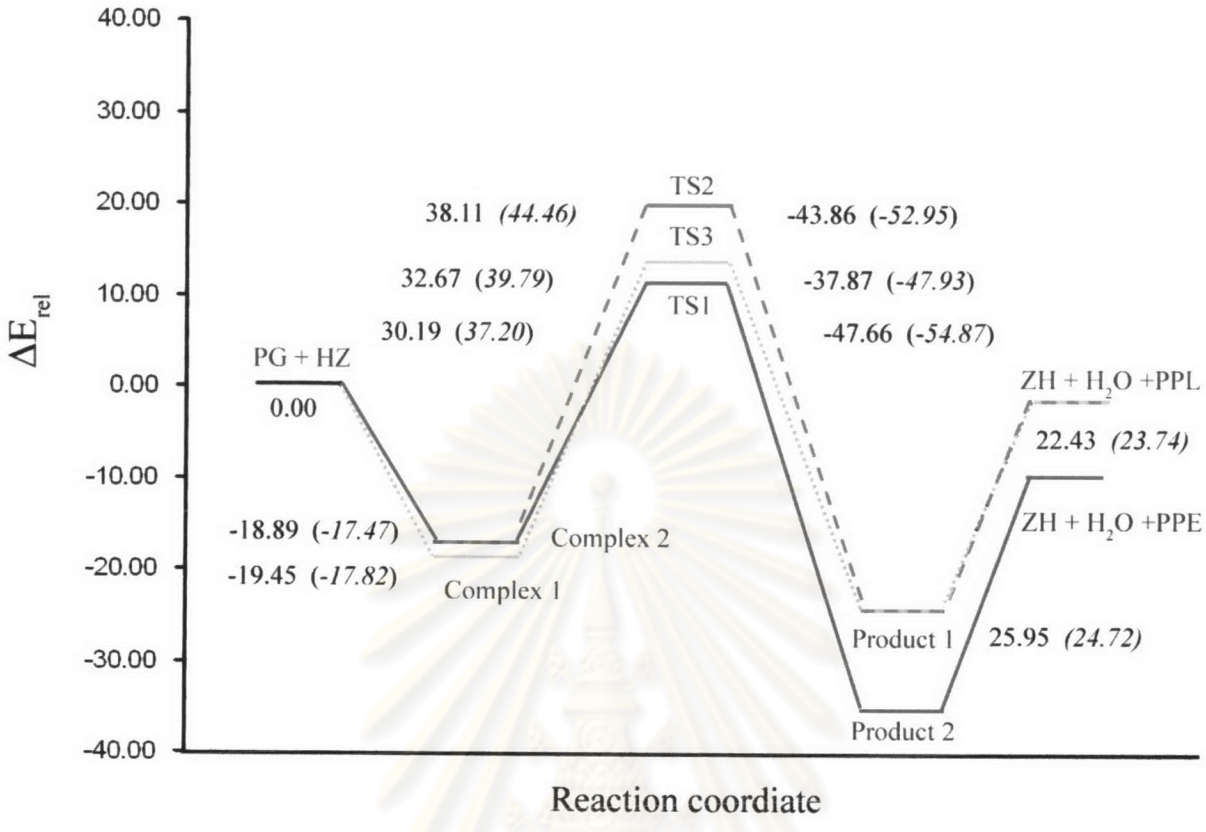

Figure 4.24 Relative energetic profiles of conversion reactions of 3T (in parentheses) and 5T (plan number) cluster models. All energies (in kcal/mol) are based upon total energies with respect to reactant PG + HZ computed at B3LYP/6-31G(d) level of theory with zero-point energy correction.

Table 4.13 Activation thermodynamic quantities and rate constants of pinacol rearrangement of propylene glycol catalyzed by zeolite cluster 3T and 5T [a].

Reaction	$\Delta^{\ddagger}E^{O}$, [b]	$\Delta^{\ddagger}H^{O}$, [b]	$\Delta^{\ddagger}G^{O}$, [b]	$\Delta^{\ddagger}S^{O}$, [c]	k, [d]
C2H pathway					
k_1^f : Complex 1 $\longrightarrow$ TS1	32.67 (39.79)	32.56 (39.92)	34.06 (40.80)	-5.02 (-2.95)	6.69×10^{-13} (7.71×10^{-18})
k_1^b : Product 1 $\longrightarrow$ TS1	37.87 (47.93)	37.18 (46.95)	39.21 (49.99)	-6.82 (-10.18)	1.11×10^{-16} (1.40×10^{-24})
C1Me pathway					
k_2^f : Complex 2 $\longrightarrow$ TS2	38.11 (44.46	38.08 (44.51)	39.23 (45.78)	-3.85 (-4.26)	1.08×10^{-16} (1.71×10^{-21})
k_2^b : Product 1 $\longrightarrow$ TS2	43.86 (52.95)	43.14 (51.85)	45.70 (55.34)	-8.60 (-11.70)	1.95×10^{-21} (1.68×10^{-28})
C1H pathway					
k_3^f : Complex 2 $\longrightarrow$ TS3	30.19 (37.20)	29.87 (37.03)	31.90 (38.59)	-6.82 (-5.23)	2.54×10^{-11} (3.19×10^{-16})
k_3^b : Product 1 $\longrightarrow$ TS3	47.66 (54.87)	46.71 (53.59)	49.45 (57.04)	-9.18 (-11.56)	3.50×10^{-24} (9.53×10^{-30})

[a] in parentheses are values from cluster 3T, plain numbers are from cluster 5T. [b] in kcal/mol. [c] in cal/mol K. [d] forward (k^f) and backward (k^b) rate constants.

Table 4.14 Percent ratio of product compositions of PPNL and PPNE from zeolite catalyzed and its ratio based upon the B3LYP/6-31G(d) computation.

Model	[PPNL] [a]	[PPNE] [a]	[PPNL]:[PPNE] [b]
3T	2.36	97.64	0.02
5T	2.56	97.44	0.03

[a] in percent. [b] Computed using equation 3.3

4.2 Pinacol Rearrangement Reaction

In this study, three catalytic systems investigated in pinacol rearrangement are acid catalyst, zeolite cluster and metal substituted molecular sieve. The results are discussed below.

4.2.1 Acid Catalyzed Reaction

All structures of pinacol rearrangement reaction in acid catalyst were optimized using DFT at B3LYP/6-31G(d) level of theory. The zero point energies and thermodynamic quantities of activation steps were derived from the frequency calculations at 298.15 K at the same level of theory. When oxygen atom of pinacol is protonated, methyl group migration is occurred. Propylene glycol is asymmetric diol, but pinacol is symmetry molecule. When the pinacol is dehydrated, the migration is occurred only one pathway that is methyl group migration while three pathways of migrations occurred for propylene glycol, as described in chapter I. Thus the pinacol rearrangement in acid catalyst is studied only one model. The electrostatic potential energies of pinacol and pinacolone are shown in Figures 4.25 and 4.26, respectively. Positive potential (blue region) of pinacol is located on the hydrogen atom of OH group while negative potential (red region) is located on oxygen atom. For the product of the reaction, pinacolone, there is slightly positive potential because the molecule has not any acidic site.

Optimized geometries and bond distances of pinacol rearrangement are shown in Figure 4.27. Relative energetic profile of this reaction is presented in Figure 4.28 Activation energy of pinacol rearrangement in acid catalyst is 14.13 kcal/mol and thermodynamic quantities are reported in Table 4.15.

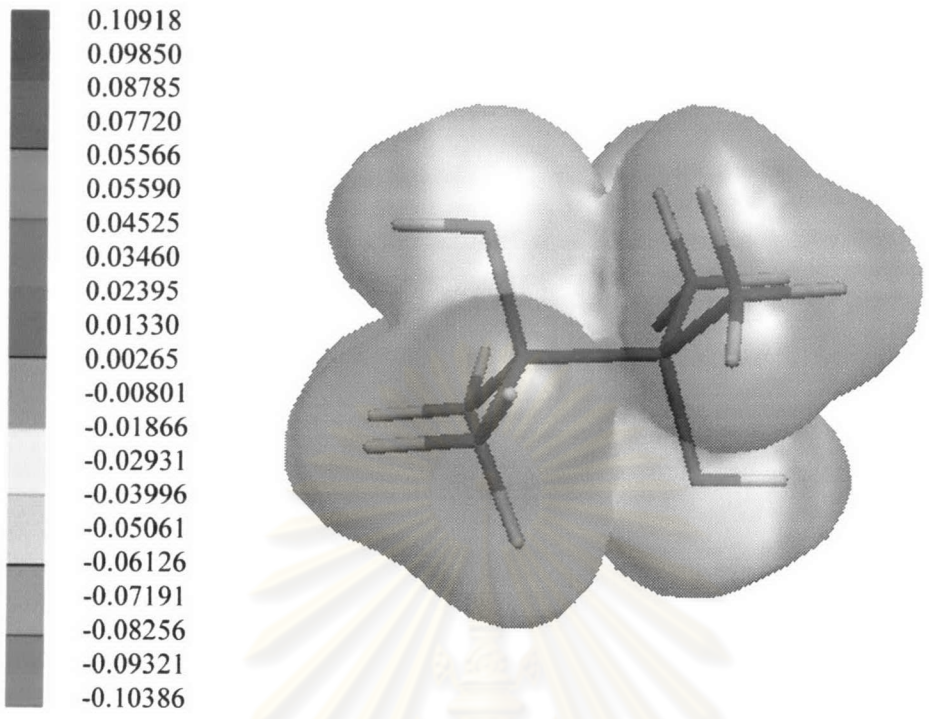

Figure 4.25 Molecular electrostatic potential energy of pinacol.

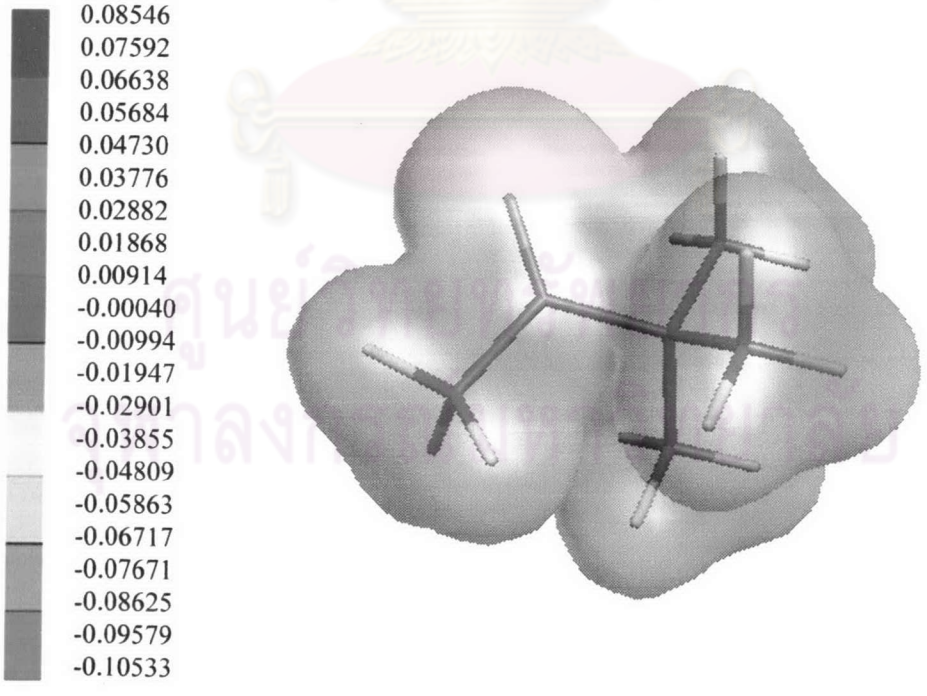

Figure 4.26 Molecular electrostatic potential energy of pinacolone.

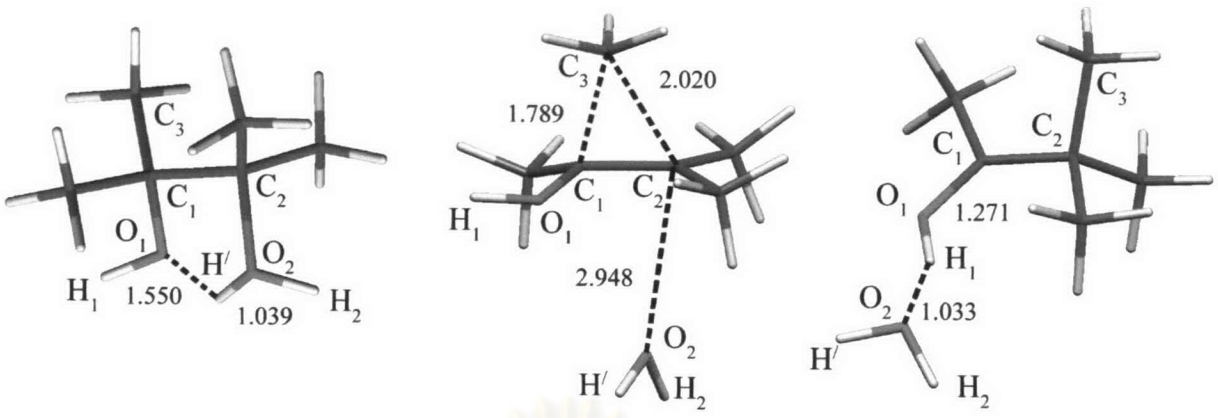

Protonated Pinacol (**HPC$^+$**) | **TS** | **Protonated Pinacolone** (**HPCL$^+$**)

Figure 4.27 The optimized geometries of pinacol rearrangement in acid catalyst. Bond distances are reported in angstroms.

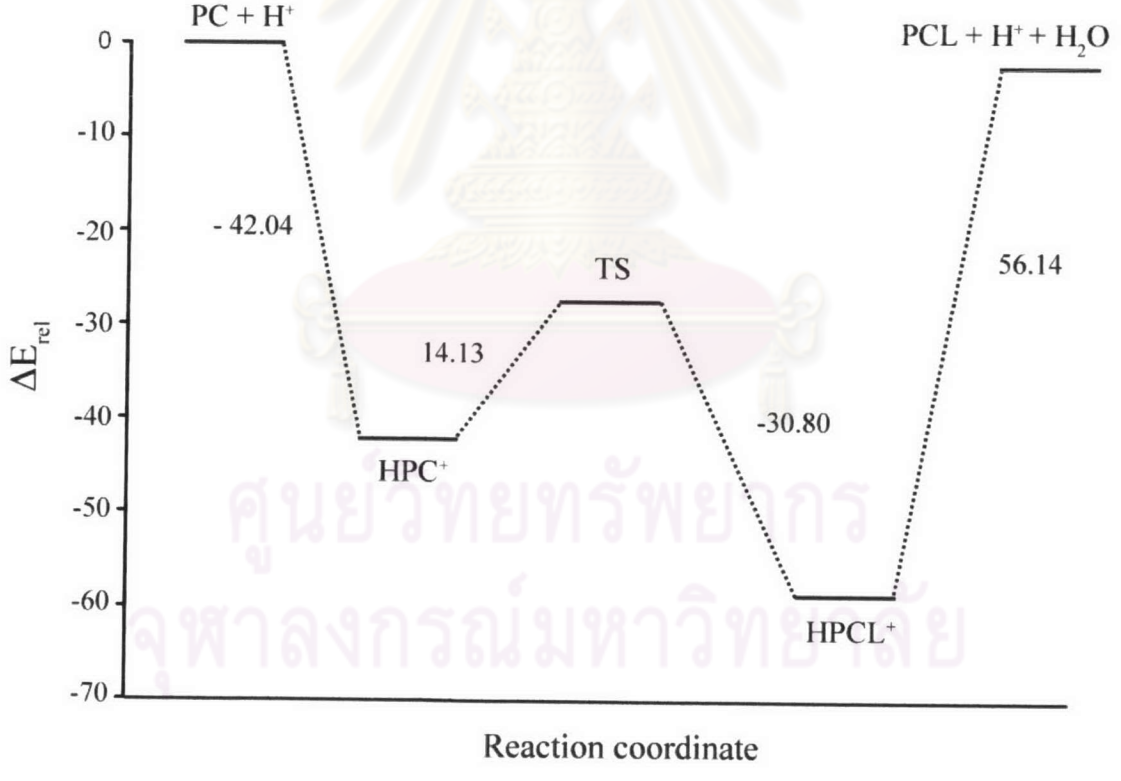

Figure 4.28 Relative energetic profile of pinacol rearrangement in acid catalyst. All energies (in kcal/mol) are based upon total energies with respect to reactant, PC + H^+, computed at B3LYP/6-31G(d) level of theory with zero-point energy corrections.

4.2.2 Zeolite HZSM-5 Catalyst

All structures of pinacol rearrangement reaction in zeolite cluster models, 3T and 5T, were optimized using DFT at B3LYP/6-31G(d) level of theory. The zero point energies and thermodynamic quantities of activation steps were derived from the frequency calculations at 298.15 K at the same level of theory. Optimized geometries and bond distances of pinacol rearrangement in 3T and 5T cluster model are shown in Figure 4.29. Relative energetic profiles of pinacol rearrangement in 3T and 5T cluster models are shown in Figure 4.30. The calculation from 3T and 5T cluster models provides quite similar not only structural parameter but also relative energetic profiles. The overall activation thermodynamic quantities and rate constants of pinacol rearrangement are shown in Table 4.15.

Table 4.15 Activation thermodynamic quantities and rate constants of pinacol rearrangement in acid catalyst, 3T and 5T cluster models.

Reaction	$\Delta^{\ddagger}E^{O}$,[a]	$\Delta^{\ddagger}H^{O}$,[a]	$\Delta^{\ddagger}G^{O}$,[a]	$\Delta^{\ddagger}S^{O}$,[b]	k,[c]
Acid catalyst					
k^{f} : HPC^{+} → TS	14.13	15.86	11.38	15.05	2.34×10^{4}
k^{b} : $HPCL^{+}$ → TS	30.80	31.09	30.92	0.58	1.34×10^{-10}
3T cluster					
k^{f} : Complex → TS	31.31	31.74	31.16	1.94	8.93×10^{-11}
k^{b} : Product → TS	40.42	39.79	41.99	-7.40	1.02×10^{-18}
5T cluster					
k^{f} : Complex → TS	31.99	32.50	32.48	0.06	9.53×10^{-12}
k^{b} : Product → TS	40.36	40.25	41.49	-4.16	2.37×10^{-18}

[a] in kcal/mol. [b] in cal/mol K. [c] forward (k^{f}) and backward (k^{b}) rate constants.

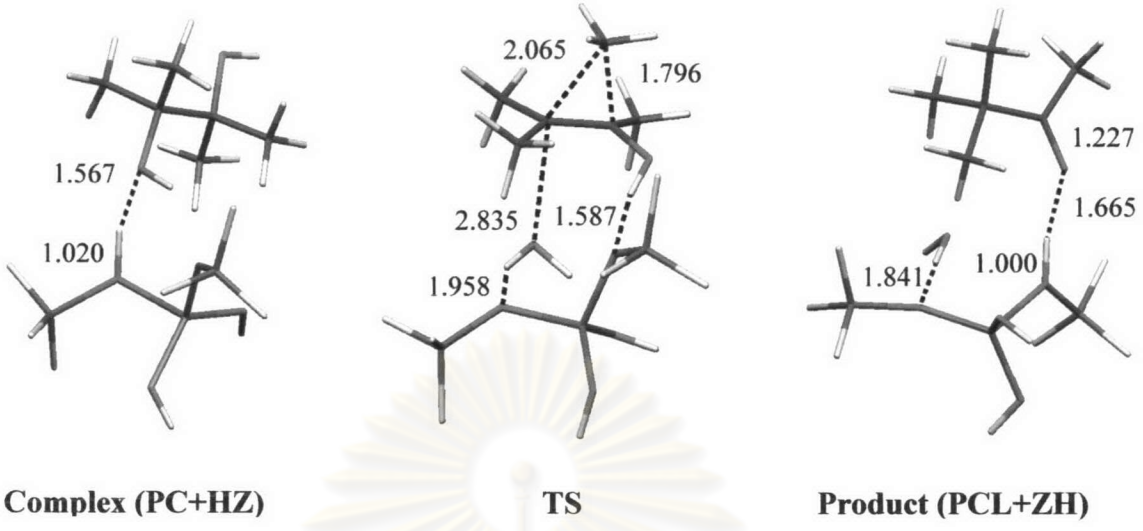

(a)

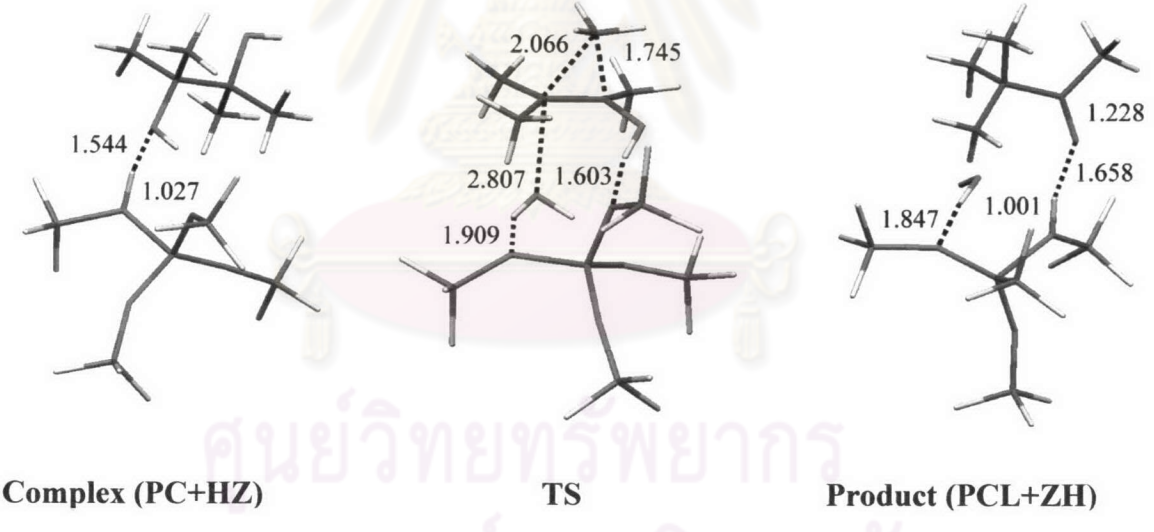

(b)

Figure 4.29 The optimized geometries of pinacol rearrangement in zeolite catalyst , (a) 3T and (b) 5T. Bond distances are reported in angstroms.

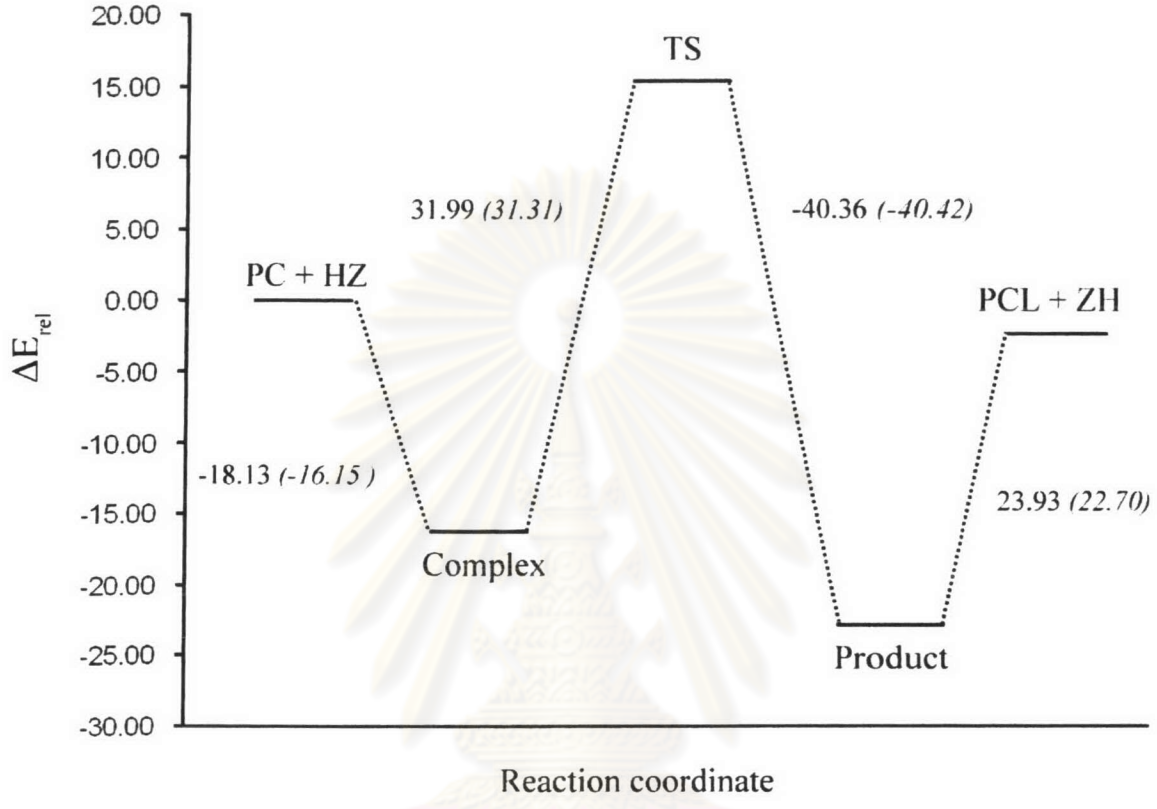

Figure 4.30 Relative energetic profiles of pinacol rearrangement over 3T (in parentheses) and 5T (plan number) cluster models. All energies (in kcal/mol) are based upon total energies with respect to reactant PC + HZ computed at B3LYP/6-31G(d) level of theory with zero-point energy corrections.

4.2.3 Metal Substituted Molecular Sieve

For metal substituted molecular sieve section, Fe- and Cu-ZSM-5 catalysts for pinacol rearrangement were investigated. All structures were optimized using DFT at B3LYP/6-31G(d) level of theory. The zero point energies and thermodynamic quantities of activation steps were derived from the frequency calculations at 298.15 K at the same level of theory. Fe- and Cu-ZSM-5 catalysts were modeled by using Fe- and Cu-3T cluster models of zeolite where Fe and Cu atoms are set on bridge between two oxygen atoms of 3T zeolite models as shown in Figure 4.31. That picture provides not only structural geometries but also presented molecular electrostatic potential energies of Fe- and Cu-3T models. The lowest electrostatic potential (red region) is in the proximity of the lone pair of the oxygen atoms, whereas the positive potential (blue region) is located in metal atom, Fe and Cu, which represent the positive charge of Fe and Cu. This study is considered the quintet spin state for Fe(II) substituted in zeolite ZSM-5 and doublet spin state for Cu(II). The result form the calculations show that the spin density on the Fe ion equals to 3.773, while those of Cu ion equal to 0.698. The atomic charges on Fe and Cu ions are 1.125 and 1.002, respectively. The atomic charges and spin densities of Fe and Cu in this study is listed in Table 4.16. These charges and spin densities of all atoms correspond to their oxidation states.

Table 4.16 Computed atomic charges and spin densities on a model of Fe-3T and Cu-3T cluster models.

Atom	Fe(II), quintet		Cu(II), doublet	
	Atomic charge [a]	Spin density [a]	Atomic charge [a]	Spin density [a]
Metal	1.125	3.773	1.002	0.698
O	-0.849	0.092	-0.799	0.125
Si	0.670	0.007	0.656	-0.002
Al	1.088	0.003	1.102	-0.006

[a] from Mulliken atomic charges and Mulliken atomic spin densities.

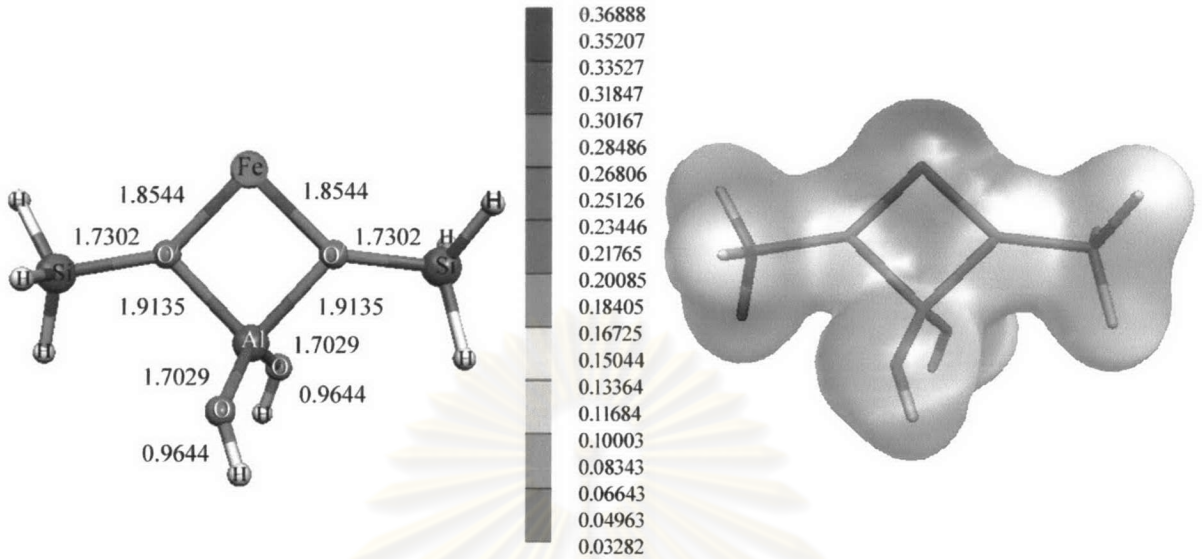

(a) Fe-3T cluster model

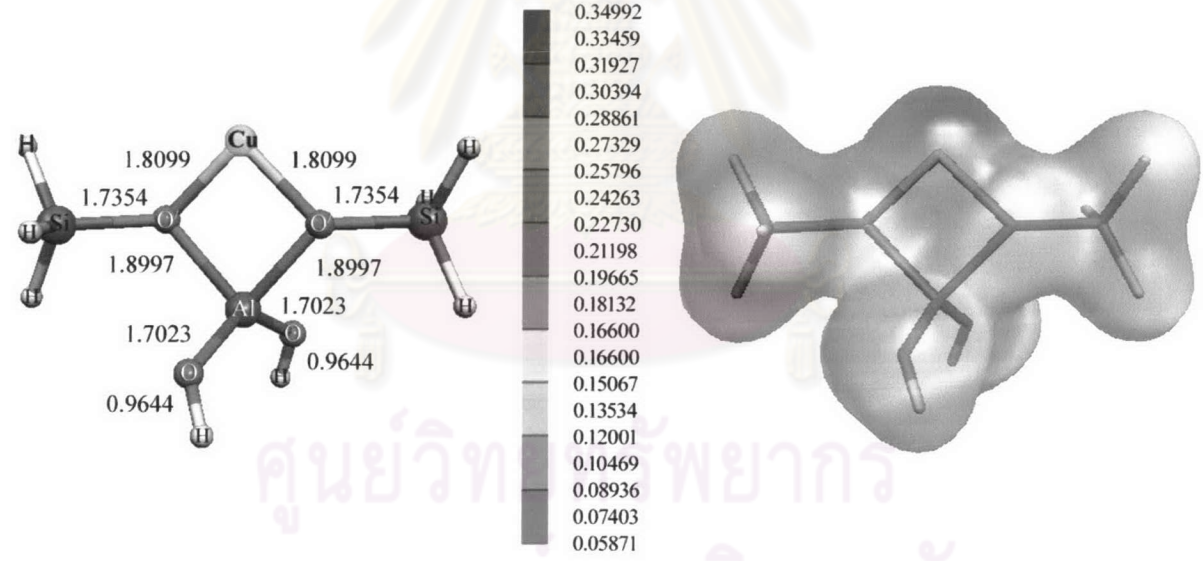

(b) Cu-3T cluster model

Figure 4.31 The structural geometries and electrostatic potential energies of (a) Fe-3T and (b) Cu-3T cluster models. Bond distances are reported in angstroms.

Optimized geometries and bond distances of pinacol rearrangement over Fe and Cu-ZSM-5 catalysts are shown in Figure 4.32 and Figure 4.33, respectively. The geometrical parameters of pinacol rearrangement over Fe-3T cluster models are shown in Table 4.17. It can be observed that reaction mechanisms of pinacol rearrangement over Fe- and Cu-3T cluster models are different from the reaction over normal zeolite and acid catalyst in aqueous phase. Because reaction in Fe and Cu substituted in zeolite framework does not involve the acid proton of zeolite, but it involves in the positive charge of metal. The mechanism of pinacol rearrangement over metal substituted in zeolite framework can be explained by using Fe-3T cluster model as an example, see detail below.

First of all, when pinacol is adsorbed on the Fe(II) active site, the positive charge of the Fe induces the lone pair of oxygen atom to form complex A. Then, the oxygen atom is donated its lone pair electron to form bond with the Fe(II) atom. This makes the proton of OH group becomes more acidic and easily transfer to the vicinal OH group in pinacol molecule by the TS1. Thus, formation of Fe-O bond facilitates the dehydration of coordinated pinacol. The water molecule is coordinated to Fe(II) and methyl group migration is occurred, present by TS2. When TS2 is finished, the electron pair on the oxygen of O-Fe(II) back-donates to the C-O bond. The final complex is the coordinated form of pinacolone and water molecule to Fe(II) atom, called complex B. For the pinacol rearrangement over Cu-3T cluster model, the reaction mechanism can be explained in the same way.

The overall activation thermodynamic quantities and rate constants of pinacol rearrangement are presented in Table 4.18. It can be observed that the highest positive relative energy is the relative energy between the complex A and TS1. Thus, the TS1 is the rate determining step in pinacol rearrangement over Fe- and Cu-3T cluster models. Rate constants for pinacol rearrangement over Fe- and Cu-3T cluster models equal 3.07×10^{-12} and 1.40×10^{-16}, respectively. Thus, the activation energy of pinacol rearrangement over Fe-3T is lower than reaction over Cu-3T. This result is in good agreement with the result from the experiment data *[1]*. For uncomplicated comparison, relative energy profiles of pinacol rearrangement in Fe- and Cu-ZSM-5 catalysts are shown in Figure 4.34 and Figure 4.35, respectively.

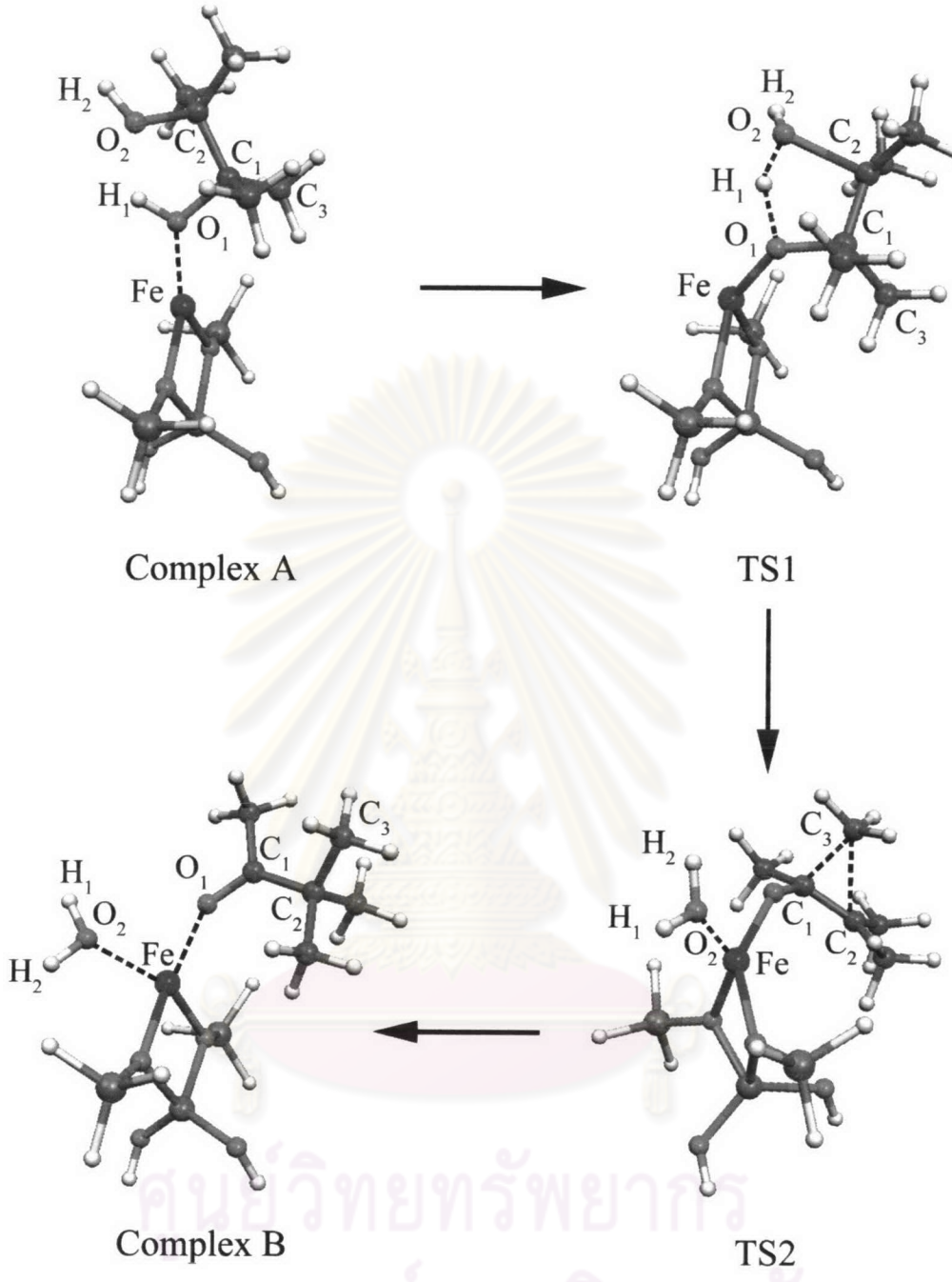

Figure 4.32 The structural geometries of pinacol rearrangement over Fe-substituted in framework of zeolite, modeled by Fe-3T cluster model.

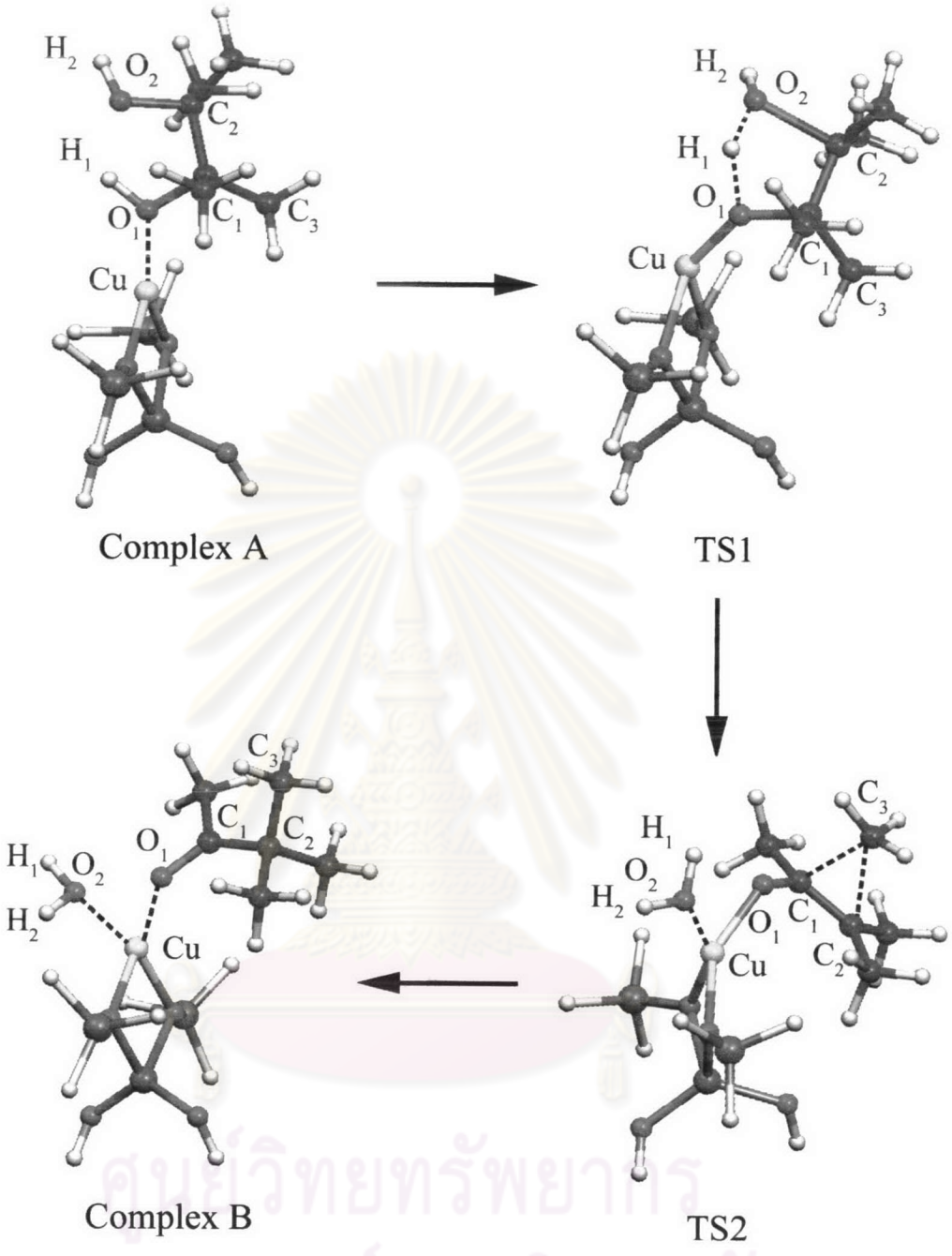

Figure 4.33 The structural geometries of pinacol rearrangement over Cu-substituted in framework of zeolite, modeled by Cu-3T cluster model.

Table 4.17 Selected geometrical parameters (bond distances and bond angles) of pinacol rearrangement over Fe-3T cluster model.

System/parameter	Reaction state			
	Complex A	TS1	TS2	Complex B
Fe-3T				
r (Fe – O_1) [a]	1.9380	1.9131	1.8790	1.9823
r (Fe – O_2) [a]	-	-	2.0895	2.0924
r (C_1 – C_2) [a]	1.5700	1.5413	1.4477	1.5187
r (C_1 – O_1) [a]	1.0596	1.4568	1.3475	1.2486
r (C_2 – O_2) [a]	1.4572	1.8642	-	-
r (O_1 – H_1) [a]	0.9986	1.3554	-	-
r (O_2 – H_1) [a]	-	1.0985	0.9712	0.9714
r (O_2 – H_2) [a]	0.9709	0.9761	0.9715	0.9736
r (Fe – O′) [a]	1.8799	1.8349	1.8419	1.9661
α (O′ – Fe – O′) [b]	84.520	78.722	79.026	81.319
α (O′ – Al – O′) [b]	86.060	89.772	88.541	87.208
Cu-3T				
r (Cu – O_1) [a]	1.8582	1.8300	1.8678	1.9252
r (Cu – O_2) [a]	-	-	2.0069	1.9949
r (C_1 – C_2) [a]	1.5694	1.5413	1.4388	1.5207
r (C_1 – O_1) [a]	1.5060	1.4568	1.3303	1.2482
r (C_2 – O_2) [a]	1.4555	1.8642	-	-
r (O_1 – H_1) [a]	0.9962	1.3540	-	-
r (O_2 – H_1) [a]	1.7559	1.0985	0.9711	0.9762
r (O_2 – H_2) [a]	0.9709	0.9761	0.9715	0.9723
r (Cu – O′) [a]	1.8639	2.0601	1.9285	1.9184
α (O′ – Cu – O′) [b]	84.286	76.674	81.327	81.939
α (O′ – Al – O′) [b]	83.790	89.772	86.203	85.322

[a] Bond distance, in angstroms. [b] Angle, in degrees.

Table 4.18 Activation thermodynamic quantities and rate constants of pinacol rearrangement in acid catalyst, Fe-3T and Cu-3T cluster models.

Reaction	$\Delta^{\ddagger}E^{O}$,[a]	$\Delta^{\ddagger}H^{O}$,[a]	$\Delta^{\ddagger}G^{O}$,[a]	$\Delta^{\ddagger}S^{O}$,[b]	k
Fe-3T cluster model					
Complex A → TS1	29.63	28.75	33.16	-14.76	3.07×10^{-12}
TS1 → TS2	-20.12	-18.16	-22.92	15.97	-
TS2 → Complex B	-34.47	-34.39	-35.23	2.80	-
Cu-3T cluster model					
Complex A → TS1	37.11	36.53	39.08	-8.56	1.40×10^{-16}
TS1 → TS2	-28.68	-27.17	-30.04	9.66	-
TS2 → Complex B	-36.01	-36.17	-36.27	0.35	-

[a] in kcal/mol. [b] in cal/mol K.

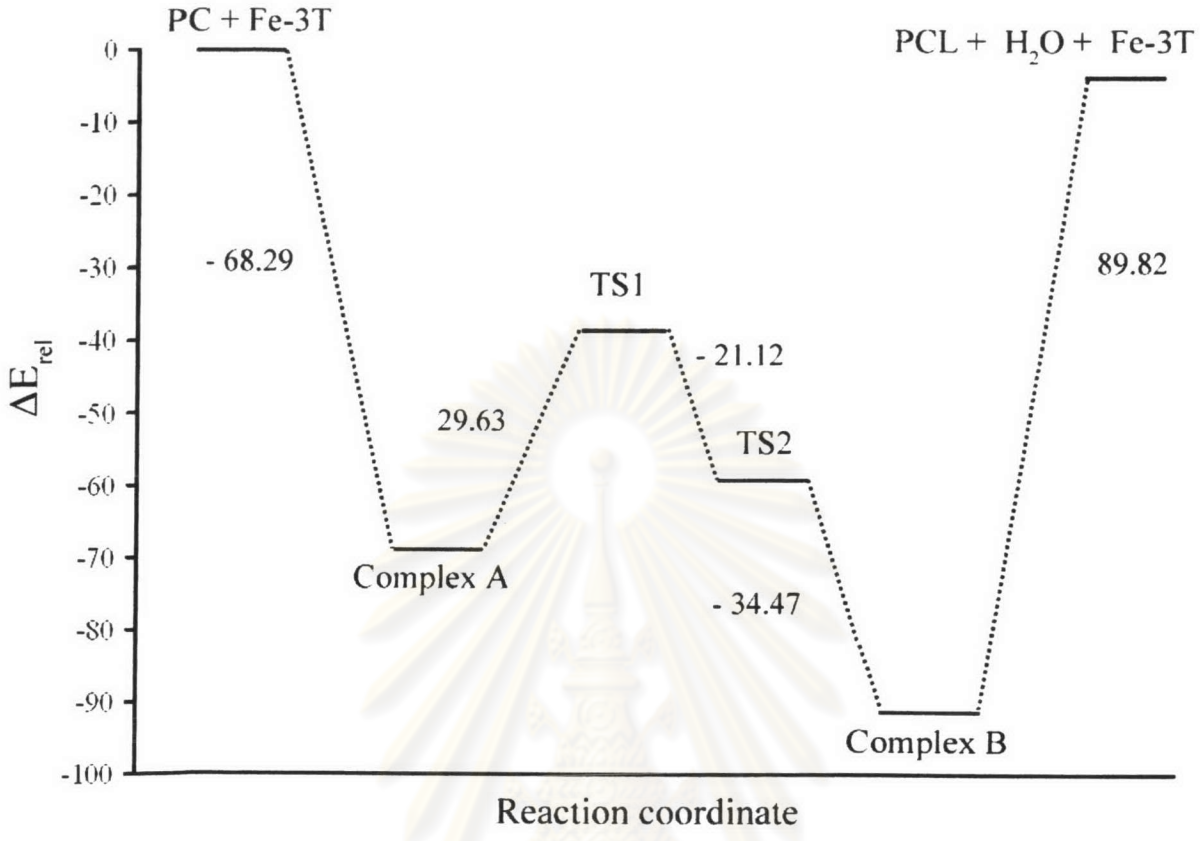

Figure 4.34 Relative energetic profiles of pinacol rearrangement over Fe-3T cluster model. All energies (in kcal/mol) are based upon total energies with respect to reactants, PC + Fe-3T, computed at B3LYP/6-31G(d) level of theory with zero-point energy corrections.

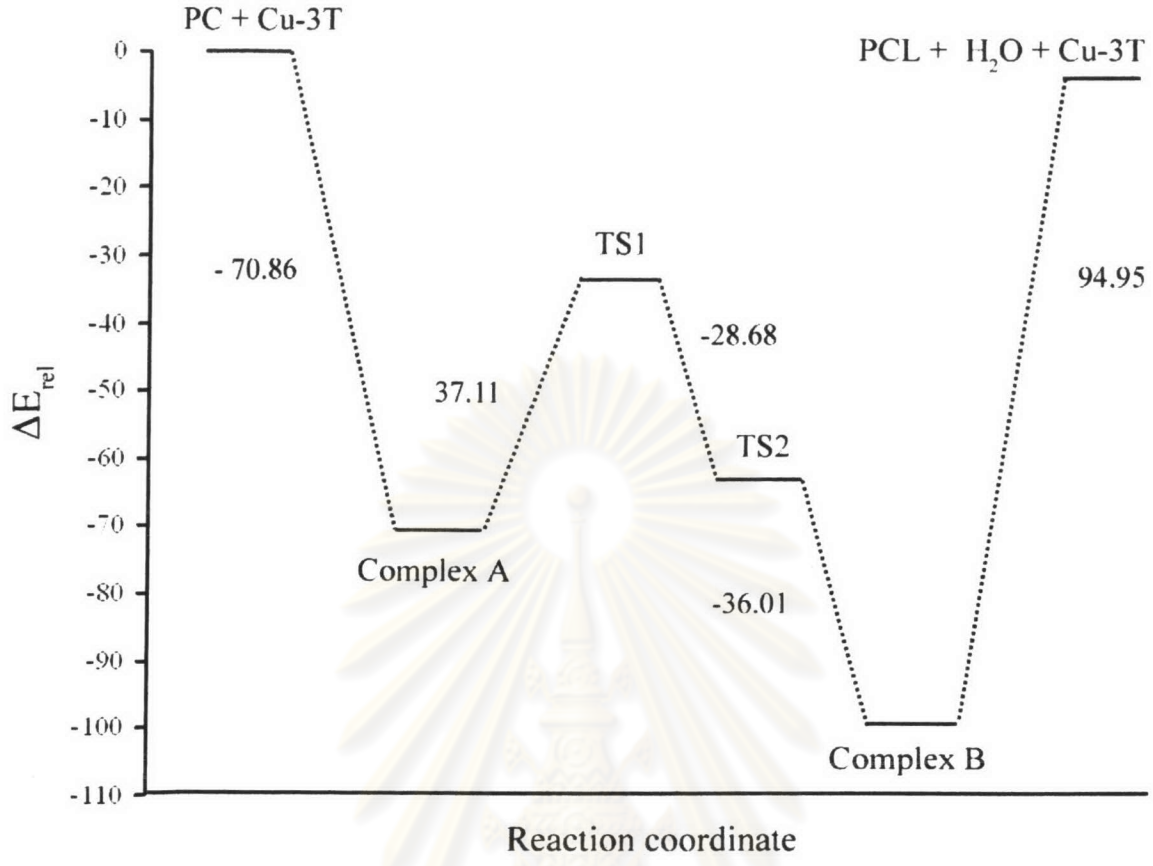

Figure 4.35 Relative energetic profiles of pinacol rearrangement over Cu-3T cluster model. All energies (in kcal/mol) are based upon total energies with respect to reactants, PC + Cu-3T, computed at B3LYP/6-31G(d) level of theory with zero-point energy corrections.